Antennas and propagation for body centric wireless communications at millimeter wave frequencies: a review

Alice Pellegrini, Alessio Brizzi, Liping Zhang, Khaleda Ali, Yang Hao, Xiaojie Wu, Costas Constantinou, Yuriy Nechayev, Peter S Hall, Nacer Chahat, et al.

Antennas and Propagation for Body-Centric Wireless Communications at Millimeter-Wave Frequencies: A Review

A. Pellegrini[1], A. Brizzi[1], L. Zhang[1], K. Ali[1], Y. Hao[1], X. Wu[2], C. C. Constantinou[2], Y. Nechayev[2], P. S. Hall[2], N. Chahat[3,4], M. Zhadobov[3], and R. Sauleau[3]

[1]Antennas and Electromagnetics Group, School of Electronic Engineering and Computer Science
Queen Mary, University of London
London, E1 4NS United Kingdom
E-mail: alice.pellegrini, alessio.brizzi, lianhong.zhang, khaleda.ali, yang.hao@eecs.qmul.ac.uk

[2]School of Electronic, Electrical and Computer Engineering
University of Birmingham
Edgbaston, Birmingham B15 2TT, United Kingdom
E-mail: xxw881, yin839, p.s.hall, c.constantinou@bham.ac.uk

[3]Institute of Electronics and Telecommunications of Rennes (IETR)
UMR CNRS 6164, University of Rennes 1
35042 Rennes, France
E-mail: nacer.chahat, ronan.sauleau, maxim.zhadobov@univ-rennes1.fr

[4]Jet Propulsion Laboratory (JPL)
California Institute of Technology
Pasadena, CA 91109 USA
E-mail: nacer.e.chahat@jpl.nasa.gov

Body-centric wireless communications represent a well-established field of research, with many studies and applications developed in a range of frequencies that extend from 400 MHz up to 10 GHz. However, many advantages can be found in operating such systems at millimeter-wave frequencies. For example, compact antennas suitable for body-centric applications can be obtained together with other benefits, such as higher data rates and reduced interference and

"observability." Meanwhile, numerical modeling of antennas and propagation at millimeter-wave frequencies represents a major challenge in terms of efficiency and accuracy. The aim of this paper is to provide a review of recent progresses and outstanding challenges in the field of body-centric communication at frequencies of 60 GHz and 94 GHz.

Keywords: Body-centric wireless communication; millimeter waves; numerical methods; phantoms; on-body antennas

1. Introduction

Over the past few years, an increasing interest in body-centric wireless communications has made this research field very popular. This is true not only in terms of theoretical studies, but also with the development of many devices and systems for different applications in numerous fields such as medicine and health care, military and defense, gaming and entertainment [1-8].

Previous studies have been carried out at carrier frequencies up to 10 GHz. Recently, research at millimeter-wave (mm-wave) frequencies has rapidly grown at 60 GHz and 94 GHz, with preliminary results published in the fields of antenna design, radio propagation measurements, and numerical modeling. Enhancing of communication-channel security, inter- and intra-system interference reduction, and the availability of underused spectrum make millimeter-wave frequencies particularly promising for the development of future body-centric wireless communication systems. The design of reliable and efficient BANs [body-area networks], operating at millimeter waves, requires such detailed analysis of the communication channel. Numerical simulation and measurements provide reliable and accurate results; however, there are still many issues to overcome. In terms of simulation, one of the main challenges arises from the fact that the human body becomes electrically large at the investigated frequencies, potentially making the computational burden of full-wave simulations extremely onerous. However, high-frequency techniques and carefully tailored formulation of full-wave methods seem to be very promising for channel characterization. In addition, the availability of accurate numerical human phantoms, obtained by means of advanced imaging techniques, make simulations a powerful tool for analyzing the on-body radio channel in great detail. For example, the effects of clothing cannot be assumed to be negligible, as the majority of investigations at lower frequencies have implicitly or explicitly implied. The typical thickness of clothes, ranging from tenths of a millimeter up to a few millimeters, is comparable to the wavelength in the V and W bands (see Section 2). The effects of clothes on the propagation channel therefore have to be carefully and systematically evaluated.

On the measurement side, the choice of antenna is of primary concern. Due to the high free-space path loss at millimeter-wave frequencies, and the high oxygen-induced atmospheric attenuation in the 60 GHz range, the antenna should have a gain able to partially compensate for such losses, enhancing the achievable maximum distance between transmitter and receiver, and allowing the characterization of longer communication paths. However, directive antennas are not suitable for such purposes. Indeed, the losses due to the misalignment of the transmitter and receiver might be higher than the losses due to the presence of the human body itself, thus negating the potential benefits of high gain. In addition, the effects of the proximity of the human body on antenna performance have to be properly investigated. The presence of cables and other equipment, necessary to install the antennas on the body, may significantly affect the measured data. In general, channel measurements taken on human subjects may raise issues related to the safety of the subject itself [9]. Moreover, repeated channel-measurement setups may differ from each other, due to an imperfectly reproduced posture of the human subject. Solid, semisolid, or liquid phantoms can therefore be manufactured to mimic the electrical properties of the actual human body.

In the light of these considerations, this paper reviews the main progress to date, and summarizes the challenges in the body-centric research field at millimeter-wave frequencies. The paper is organized as follows. In Section 2, the main regulations and the reasons that make millimeter-wave frequencies both appropriate and desirable for use in body-centric wireless systems are provided. Section 3 reviews the numerical methods available for analyzing on-body links at millimeter-wave frequencies. A discussion of numerical and experimental phantoms is presented in Section 4, while Section 5 reviews the state of the art for antennas for body-centric applications. Finally, an overview of channel-characterization studies is provided in Section 6.

2. The Millimeter-Wave Band

Generally, the range of frequencies associated with *millimeter waves* covers the band between 30 GHz and 300 GHz. Nevertheless, when referring to telecommunications, this term usually describes the sub-bands around 60 GHz, 70 GHz, 80 GHz and 90 GHz, since these are the portions of the spectrum allocated for public use in various countries [10]. Due to the lack of an officially accepted definition, these sub-bands will be henceforth referred to as mmW-60, mmW-70, mmW-80 and mmW-90, respectively.

The allocation of such frequencies began in 1995, with the release by FCC of the bands between 59 GHz and 64 GHz (subsequently extended from 57 GHz to 64 GHz) for commercial wireless application, followed by 71 GHz to 76 GHz, 81 GHz to 86 GHz, and 92 GHz to 95 GHz between 2003 and 2005 (Figure 1) [11, 12]. However, according to the various national regulations, these bands are treated in different ways and have different availabilities.

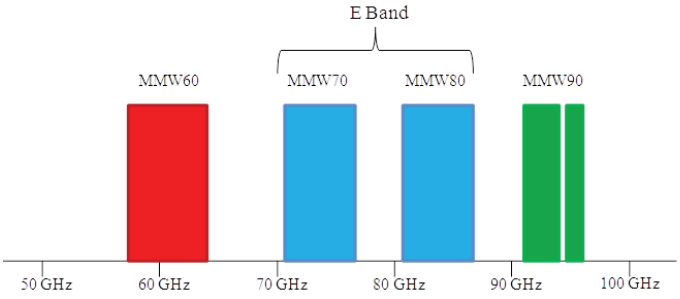

Figure 1. The bands allocated at millimeter-wave frequencies by the FCC in the US [11, 12].

In particular, mmW-60 is regulated by the FCC Code of Federal Regulation (CFR), Title 47, Part 15, for unlicensed operations [13], meaning that no application for license has to be made prior to the deployment of a service operating in this band. MmW-70 and mmW-80 are instead governed by CFR Title 47, Part 101 [14], for licensed operation. In particular, non-government bodies are allowed to apply for the registration of non-exclusive nationwide licenses for point-to-point and non-broadcast services. Potential users may apply for licenses covering the whole 5 GHz spectrum available in each of these two bands, as well as just for a portion of it. The 5 GHz of spectrum available in each of the mmW-70 and mmW-80 bands can therefore be used as a single, contiguous transmission channel, with no channelization requirements.

Finally, it is worth mentioning that the mmW-90 band has a peculiar regulation. It includes a 100 MHz exclusion band between 94 GHz and 94.1 GHz that can be used exclusively for space research services and Earth exploration satellite services [11]. Moreover, its unlicensed use under CFR, Title 47, Part 15, is allowed only for indoor applications. At the moment, this poses some limitations on the on-body communication systems that can be developed in the mmW-90 band, although most medical and home-entertainment applications would comply with the above-mentioned rule by their own nature. MmW-90 can also be used for outdoor point-to-point links, but in this case, it falls under CFR Title 47, Part 101, in the same way as do mmW-70 and mmW-80.

Apart from the US, the scenario in the rest of the world is extremely varied at the present time. A reasonably good agreement among various national regulating bodies can be found only for the mmW-60 band [15]. The band plans and rules for various countries are summarized in Table 1. A summary of regulations and features of lower frequencies for body-centric communication can be found in [16]. A summary of the available worldwide mmW-70, mmW-80, and mmW-90 bands [22, 23] is reported in Table 2.

These four frequency bands give rise to different levels of interest for the development of future BANs. MmW-70 and mmW-80 are highly interesting as alternatives to fiber optics for Gb/s long-range point-to-point communications. In fact,

Table 1. The regulation of unlicensed bands around 60 GHz.

Region	Frequencies [GHz]	Max Transmitted Power [mW]	Max Antenna Gain [dBi]
USA [13]	57-64	500	Not Specified
Canada [17]	57-64	500	Not Specified
Japan [18]	59-66	10	47
EU [19]	57-66	20	37
Australia [20]	59.4-62.9	10	47
South Korea [21]	57-64	10	TBD

Table 2. The worldwide availability of millimeter-wave frequency bands.

Band	MMW70	MMW80	MMW90
Frequency Range (GHz)	71-76	81-86	92-95 (US only)

various companies – such as AMS Technologies [23], Ceragon [24], and Bridgewave [25] – are already offering 70/80 GHz wireless backhaul solutions. Any BAN application developed in the mmW-70 and mm-80 bands would therefore be forced to compete with these existing services in terms of band usage.

On the other hand, the reduced risk of competition with wireless backhaul services instead makes the mmW-60 and mmW-90 bands more interesting for body-centric applications. The same regulation of mmW-60 has been applied by the FCC to indoor applications working at mmW-90. This allows cost limitations and greater flexibility in the design of millimeter-wave body-centric systems. In addition, losses due to the atmospheric absorption at the considered frequencies are negligible for the distances typically associated with body-centric communications. In contrast, free-space path losses – evaluated according to the formula $20\log\left(4\pi d/\lambda\right)$ [26], with d being the distance in free space – make these frequencies less suitable for long-range links (Table 3).

3. Numerical Methods

Numerical simulations are an extremely useful tool for the investigation of radio propagation around the human body. They provide a deeper understanding of the physics behind the data collected during measurements, while not suffering from the same repeatability issues. Unlike theoretical analyses, numerical simulations do not require extreme simplifications of the human body, thus affording the simulation of very realistic and accurate scenarios.

Various numerical methods are available in the literature, each with specific advantages and drawbacks, making them suitable for handling specific classes of propagation problems. The methods that appear to be particularly promising for the analysis of body-centric propagation at millimeter-wave frequencies are discussed in the next sections.

3.1 Ray-Based Methods

When propagation and scattering involve objects the dimensions of which are several wavelengths large, high-frequency asymptotic techniques provide computationally efficient, accurate solutions. Considerable attention has been dedicated to ray-based techniques for their implementation simplicity and ease of ability to be hybridized with other methods.

In Geometrical Optics (GO), reflected and refracted fields from and through surfaces are calculated according to the generalized Fermat law, and their contributions are added to the incident field to calculate the total field at a certain point in space. Although this method is able to very efficiently take into account multiple reflections and transmissions, it ignores the diffraction contributions from edges and curved surfaces. Such contributions can be calculated by means of the Uniform Theory of Diffraction (UTD) [27]. The combined use of Geometrical Optics and the Uniform Theory of Diffraction provides a powerful tool for investigating electrically large objects with good accuracy and limited computational effort. A further advantage of ray-based techniques is their ability to accurately and efficiently predict parameters such as the power delay profile (PDP) and the delay spread (DS). For this reason, ray-based techniques have been widely used in the electromagnetic analysis of indoor and urban outdoor scenarios, especially for the evaluation of signal coverage for mobile phones and other wireless networks [26, 28, 29]. Ray-based techniques have also been used to model the effects of the human presence on the indoor propagation channel [30, 31].

Ray-based methods have recently been explored for the analysis of body-centric scenarios. Indeed, the human body is electrically large at millimeter-wave frequencies, and full-wave techniques are computationally inefficient in solving equations with a high number of unknowns. Cotton et al. [8] used a ray-based method to analyze short-range soldier-to-soldier communications at 60 GHz. The use of Geometrical Optics/ Uniform Theory of Diffraction for on-body propagation was also investigated in [32].

Several studies have been presented for evaluating the prediction accuracy of ray-based techniques applied to on-body communication [33-35]. Specifically, three-dimensional numerical models composed of facets were considered, the electromagnetic properties of human tissues and fabrics were defined, and the radiation patterns of the antennas were applied to the transmitter and receiver, as indicated in Figure 2a. Figure 2b shows the ray-optical paths computed in this

Table 3. Atmospheric absorption and free-space path loss at 94 GHz and 60 GHz for body-centric communication Links.

Communications Range [m]	Atmospheric Absorption [dB]		Free-Space Path Loss [dB]	
	94 GHz	60 GHz	94 GHz	60 GHz
0.3	1.5e-4	6e-3	61	58
1	5e-4	2e-2	72	68
5	2.5e-3	1e-1	86	82
10	5e-3	2	92	88

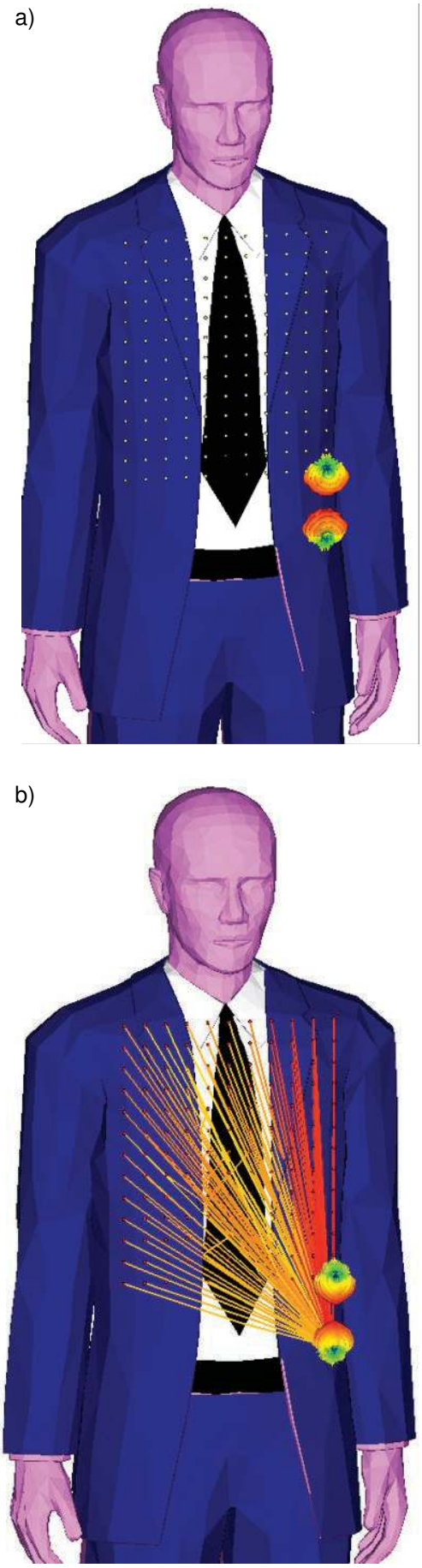

Figure 2. A possible simulation setup (a), and ray tracing paths on the waist-to-chest link (b).

model when considering direct-, reflected-, and diffracted-ray contributions.

Comparisons among measurements carried out on a real human subject and simulations performed on several numerical phantoms were provided for different links, as will be shown in Section 6 of this paper. According to these studies, ray-based techniques are sufficiently reliable for analyzing wireless body-centric communication-link scenarios. However, several factors, such as the modified radiation pattern of the antennas placed in proximity to the human body, and mechanisms of guided propagation through the clothing layers, have to be carefully taken into account.

3.2 Finite-Difference Time-Domain (FDTD)

Introduced by Yee in 1966 [36], the Finite-Difference Time-Domain method has quickly become the preferred technique for the analysis of on-body and intra-body propagation at frequencies up to X band [37-42]. The FDTD is based on the iterative solution of the discretized Maxwell's equations in the time domain [43]. It has several advantages that make it highly suitable for addressing propagation scenarios involving the human body. The FDTD is able to handle inhomogeneous media very efficiently, and its computational complexity is $O(N)$, where other methods have an $O\left[N\log(N)\right]$ complexity or higher. Scenarios involving dispersive materials can be easily analyzed. Moreover, being a time-domain method, wideband results can be obtained from only one simulation [44] by accurately defining a proper time-domain excitation source. Realistic antennas can be simulated by using the Equivalence Principle [45]. An interesting advantage of the FDTD is the possibility of being parallelized [43-47] in order to handle larger electrical problems. Indeed, as mentioned above, some of the main concerns in simulating millimeter-wave on-body links are the huge relative dimensions of the human body, consequently necessitating a very large number of discretization cells. However, the investigated geometry can be divided into sub-blocks, and each of them separately analyzed (Figure 3). On the other hand, the FDTD presents some drawbacks. The direct application of the FDTD to on-body millimeter-wave propagation is limited by the fact that the investigated volume has to be discretized with cubic cells having dimensions of $\lambda/10$ or smaller. Due to the electrically large dimensions of the human body, the number of unit cells necessary to discretize a whole human phantom is therefore of the order of 10^{11}, thus requiring computational resources that exceed most of those commercially available at the time of writing, even if a parallel implementation is used. One more limitation of the FDTD is the approximation of curved surfaces, due to the "staircasing" caused by the use of cubic cells.

However, these considerations notwithstanding, the FDTD remains a useful tool for analyzing shorter links that only require modeling a small part of the human body, as is shown in Section 6 of this paper.

a)

b)

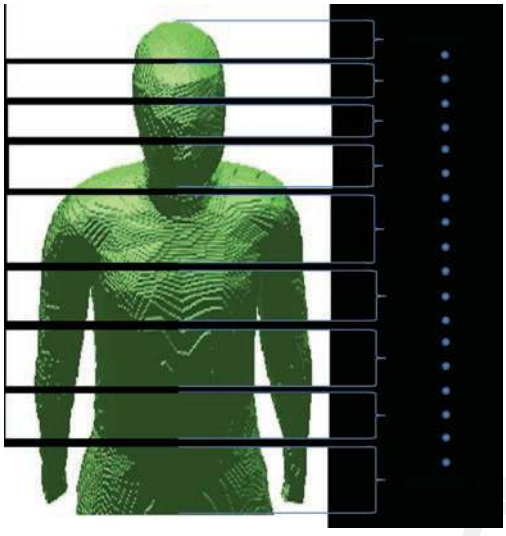

Figure 3. Th sliced human body model (a), and the parallel FDTD computational domain analyzed by several processors operating in parallel (b).

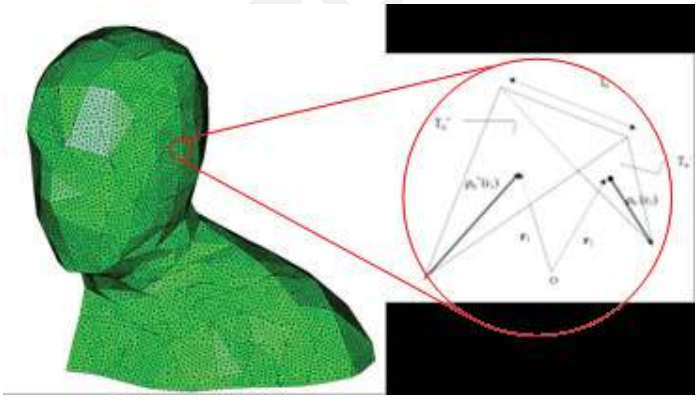

Figure 4. Triangular base functions for the MoM.

3.3 Method of Moments (MoM)

This technique is based on the solution of the integral form of Maxwell's equations over the boundaries of the investigated scenario [48]. The equations are projected over a set of basis functions, thus obtaining a linear system of equations where the unknown coefficients represent the surface currents. The most well-known formulation is the one proposed by Rao, Wilton, and Glisson [49], which uses a set of triangular basis functions to discretize the surface currents over an arbitrary surface, as depicted in Figure 4. This method is particularly efficient when dealing with domains having a high volume-to-surface ratio, since it does not require solving Maxwell's equations over all of the investigated volume. Moreover, once the surface currents have been obtained, far-field quantities, such as the radiation pattern or the radar cross section (RCS), can be directly calculated. MoM can be easily applied to structures made either of good conductors ($\sigma \gg \omega\varepsilon$) or being well described by an impedance boundary condition [50]. However, this method suffers from several disadvantages when dealing with on-body propagation. The solution of problems involving inhomogeneous media and lossy dielectrics, although possible, significantly increases the computational complexity, thus making the MoM much less efficient than other full-wave techniques. In fact, the classical MoM formulation has an $O\left(N^2\right)$ complexity and is difficult to parallelize, thus making it unable to handle electrically large objects. For these reasons, it has been applied to the analysis of on-body propagation for only a few specific problems [51-53].

4. Experimental and Numerical Human Phantoms

Measurement campaigns on human subjects are a valid and widely used tool to investigate propagation around the human body. However, they are very time consuming, are limited by the safety and comfort of the subject, and have poor repeatability. In order to overcome these issues, alternative investigation methods can be used:

- Measurements on phantoms mimicking the characteristics of human tissues;
- Numerical simulations on detailed numerical models of the human body.

These types of phantoms are described in the following subsections.

In general, electromagnetic properties of human tissues vary with frequency. In order to accurately model or manufacture human phantoms, the dispersive characteristics of different tissues therefore have to be considered, as shown in Table 4.

Table 4. The dielectric permittivities and electric conductivities of different human tissues as functions of frequency [54].

Tissue	Relative Dielectric Permittivity			Electric Conductivity [S/m]		
	94 GHz	60 GHz	2.5 GHz	94 GHz	60 GHz	2.5 GHz
Dry Skin	5.79	7.97	37.95	39.18	36.39	1.48
Muscle	9.02	12.8	52.66	61.4	52.82	1.77
Fat	2.91	3.13	5.27	3.47	2.81	0.10
Blood	8.65	12.27	58.18	62.43	54.71	2.58

4.1 Experimental Phantoms

The human body is composed of several types of tissues, which exhibit different electromagnetic properties. Accurate inhomogeneous phantoms can be manufactured by reproducing both the geometry and the electromagnetic characteristics of human tissues with the use of proper dielectric materials. In practice, designing heterogeneous phantoms is very challenging, and therefore equivalent homogeneous models have been used in most of the studies. Experimental phantoms have been extensively used at frequencies up to 11 GHz for a varied range of purposes, from the development of X-ray and magnetic-resonance imaging (MRI) applications to Specific Absorption Rate (SAR) evaluation [38]. At frequencies up to 10 GHz, homogeneous phantoms have been used to accurately evaluate antenna-parameter distortions [38, 55], and for the characterization of the propagation channel in a reproducible and well-controlled manner [56]. Usually, a weighted average of the electrical properties of the various tissues involved in the propagation or dosimetry analysis is considered [57].

However, due to the shallow penetration depth in the body at millimeter-wave frequencies [9], homogeneous skin-equivalent phantoms can be successfully used for numerical and experimental antennas and propagation studies. This is clearly demonstrated in Figure 5, which depicts the power reflection coefficient for a flat, homogeneous and a multilayer phantom.

Many different phantoms have been proposed. However, they can all be placed into one of three main categories, according to their state: liquid, semisolid, or solid phantoms.

Liquid phantoms are widely used in SAR evaluation. They consist of a container filled with a liquid exhibiting the required dielectric properties. The shape of the container is often made similar to the body or to part of it, as depicted in Figure 6. The IEEE provides recommendations for the phantoms to be used in the evaluation of SAR from handheld wireless devices [59]. To the best knowledge of the authors, liquid phantoms are only available for frequencies up to 6 GHz.

The need for a container can be avoided by using semi-solid or solid phantoms. In the former case, a coagulant agent is added to the liquid in order to create a gel-type material capable of retaining a given shape without external support. For water-based phantoms, the main disadvantage is their limited lifespan. In fact, due to the high water content, they are prone to the growth of fungi, and gradually dehydrate with a consequent degradation of their electrical properties.

The first *semisolid phantom* was proposed in [61], where a mixture of de-ionized water, sodium chloride, TX-150, and polyethylene powder was used to simulate fat and muscles between 200 MHz and 1 GHz. Other mixtures were later introduced, aimed at expanding the frequency range [62], or improving the phantom's lifespan [63]. Although the majority of the phantoms available in the literature presented accurate behaviors at frequencies up to 11 GHz, an experimental homogeneous human-skin-equivalent semisolid phantom, covering the 55-65 GHz range with $\pm 10\%$ error compared to the target values of the dry skin ($\varepsilon^* = 7.98 - j10.9$ at 60 GHz) was recently proposed in [64, 65]. The main constituents of the

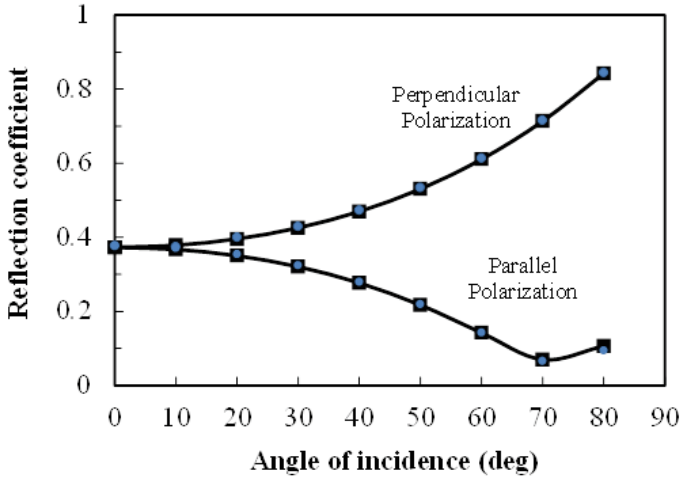

Figure 5. The computed power reflection coefficient at the air/phantom interface for different models at 60 GHz: • homogeneous skin model (with dry skin properties from [58]); —— 15 μm thick stratum corneum (SC) and underlying homogeneous skin tissue; ■ 15 μm thick SC, the rest of epidermis and dermis (1.45 mm-thick), and fat. Perpendicular (parallel) polarization denotes the E field perpendicular (parallel) to the plane of incidence.

Figure 6. Shells for liquid phantoms (reproduced from [60]).

Figure 7. A skin-equivalent phantom representing an arm and a hand: (left) a human arm used to make a realistic mold; (right) the phantom.

phantom were de-ionized water, agar, polyethylene powder, TX-151, and sodium azide (NaN_3). The phantom's complex permittivity, measured at 60 GHz, was $\varepsilon^* = 7.4 - j11.4$. Two methods were used for its characterization: a temperature-based technique [66], and a coaxial probe [64, 67]. The fabrication technique was described in detail in [65]. It allowed the production of highly realistic body-specific shapes, as illustrated in Figure 7. The lifetime of such phantoms is typically one week.

When internal field measurements are not required, dry solid phantoms can be used. They are best suited for investigating the interaction of the electromagnetic field with the body's surface, and for on-body propagation analysis. Unlike liquid and semisolid phantoms, they allow coexistence of heterogeneous tissues in the same volume.

Solid phantoms have been proposed at frequencies up to 6 GHz, based on various materials including carbon fibers and silicon rubber (Figure 8) [68], ceramic and graphite powder [69], and a conductive plastic [70]. Although they have a longer lifespan than semisolid phantoms, they are also more expensive, and require advanced complex manufacturing processes involving extremely high pressures and temperatures.

4.2 Numerical Phantoms

As already mentioned, numerical simulations are an extremely powerful tool in the analysis of body-centric communications. They require a digital representation of the human body suitable for the chosen numerical technique. They range from simple geometrical shapes, such as cylinders and parallelepipeds, to accurate geometrical models realized by means of imaging techniques. The various phantoms proposed in the literature can be divided into three main groups: volumetric, surface, and statistical phantoms.

Volumetric phantoms are the most common class of phantoms. They are usually obtained by means of MRI or computed axial tomography (CAT) scans, or by dissection of human cadavers. This allows the accurate modeling of both the shape and internal composition of the human body. The different tissues are identified, and the relevant permittivity and conductivity are subsequently assigned to each of these, as depicted in Figure 9. The volume is usually discretized into three-dimensional homogeneous unit cells called voxels (a contraction of "volumetric pixel"): the size of the voxel thus sets the resolution of the model. One of the most widely used models is Hugo [71], obtained from the corpse of a 38-year-old Caucasian, as shown in Figure 10a. This phantom has a volumetric resolution of 1 mm^3 , and has 40 different types of

Figure 8. Solid phantoms made of carbon-loaded silicon rubber (reproduced from [60]).

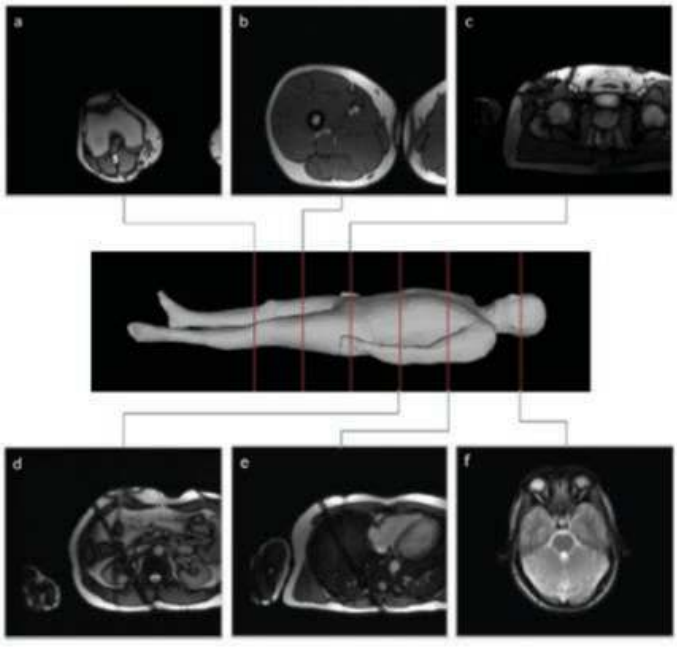

Figure 9. The generation of a human-body phantom from an MRI scan (reproduced from [72]).

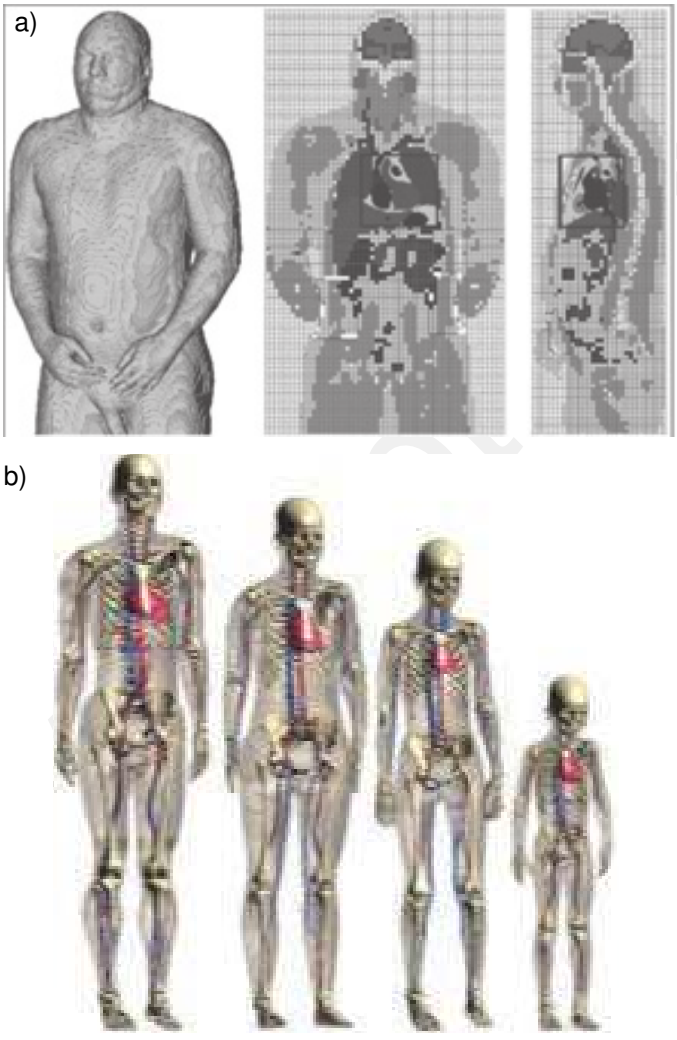

Figure 10. Volumetric human phantoms: (a) the Hugo model, and (b) the Virtual Family (reproduced from [73]).

tissues identified. Many other models are available, obtained from subjects differing in sex, age, and ethnicity, as depicted in Figure 10b. These models are particularly suited for numerical simulations with FDTD, since this technique requires the discretization of the computational domain in hexahedral cells. On the other hand, a detailed representation of the inner tissues is not necessary when analyzing the propagation around the body at millimeter-wave frequencies: as already mentioned, the electromagnetic field interacts almost exclusively with the skin layer.

Surface phantoms represent only the external surface of the human body. They can be obtained by means of laser body scanners from a human subject (Figure 11a), or by using computer-aided design (CAD) software (Figure 11b). They can also be extracted from the above-mentioned volumetric phantoms. Surface models are best suited for Method of Moment (MoM) or ray-based techniques, although a homogeneous volumetric phantom for FDTD can be obtained from a surface phantom by applying voxelization software to the latter, such *Binvox* [74].

Statistical phantoms in fact represent a particular class of surface phantoms developed by Lee et al. [72], aimed at developing a fast and inexpensive technique for generating subject-specific phantoms. Although the effects of subject-specificity on on-body propagation have been demonstrated [39], the production of a digital phantom from MRI is in fact expensive, time consuming, and often stressful for the subject. Laser scanners are faster and more comfortable, but the cost of such a system is extremely high. In order to overcome this issue, a statistical whole-body model was derived from a set of 10 male and 10 female MRI scans by using an algorithm to instantiate new surface phantoms with the parameters allowed by the training set. Five models with different sizes are shown in Figure 11c.

5. Antennas for On-Body Applications

Antennas are a key point in the design of body-centric wireless systems. They are required to guarantee a satisfactory power transfer between nodes placed on different parts of the body, as well as communication with off-body devices. On-body antennas should also be compact and light weight, possibly allowing for integration with clothes and garment accessories. However, as already proven in the 400 MHz to 10 GHz range [38], when placed on or in close proximity to the human body, antennas experience detuning, radiation-pattern distortion, and changes in the input impedance and efficiency. Hence, in order to minimize the influence of the body on antenna performance, antennas should be designed to operate robustly in close proximity to the human body.

5.1 60 GHz Wearable Antenna Requirements

Common requirements for wearable antennas consist of being low profile, light weight, and conformal to the body's

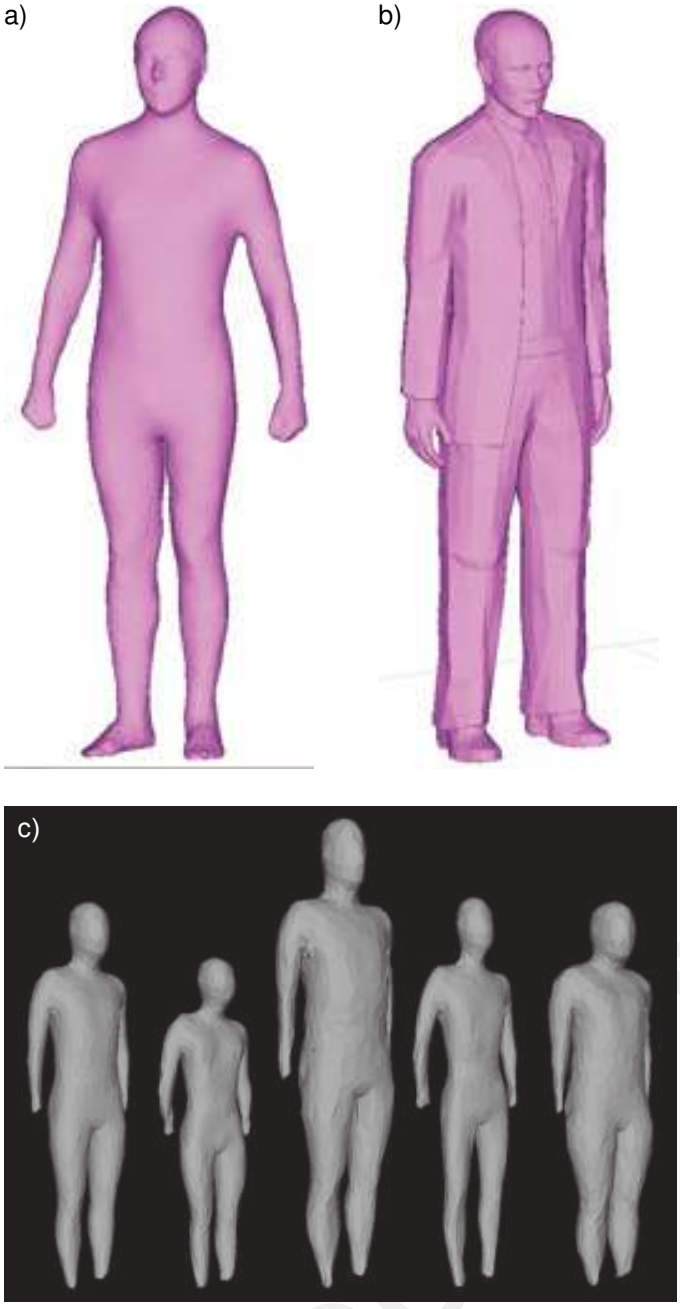

Figure 11. Surface phantoms: (a) from a laser scan, (b) from a CAD model, (c) statistical body shapes (reproduced from [72]).

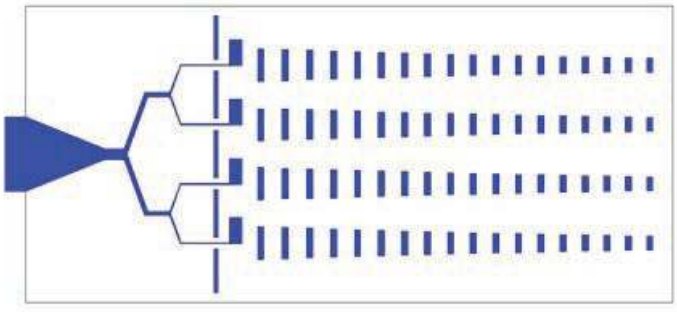

Figure 12. A bottom view of the printed Yagi-Uda array.

surface. Wearable antennas also need to be insensitive to being situated in close proximity to the human body, need to minimize the exposure of users to radiation, and need to have a radiation-pattern shape that minimizes the path-link loss [75]. At 60 GHz, the propagation losses in free space are quite high, and, according to on-body channel measurements performed by using monopole antennas, typical path losses on the human body vary between 57 dB and 88 dB, depending on the link [76]. This makes establishing a reliable communication link on a human body challenging, as the links have to be short and unobstructed. High antenna gain is therefore required to boost the signal. Based on on-body channel-measurement results and path-loss calculations, at least 10 dBi gain is required at both the transmitter and receiver for a line-of-sight path of length implied by typical human-body dimensions. For on-body communications, the maximum of the radiation pattern should be tangential to the body's surface to maximize coupling between body-worn devices, except for wearable antennas radiating outward when establishing an off-body link. Previous studies showed that a monopole antenna gives very good results for on-body applications at lower frequencies [75], but it does not provide high enough gain, required in the 60 GHz band. Metamaterial structures have been proposed to improve the gain [77]. Such high-gain antennas can lead to better security, as they minimize the amount of energy radiated away from the body, thus giving good BAN-to-BAN and BAN-to-a-fixed-base-station isolation.

5.2 Wearable Yagi-Uda Antennas for On-Body Communications

For the aforementioned reasons, Yagi-Uda antennas have been proposed as an appropriate candidate for on-body communications. In fact, they afford a good compromise in terms of size and gain performance compared to some other end-fire antennas, such as tapered-slot antennas. Figure 12 shows a printed Yagi-Uda array that consists of four single Yagi-Uda linear arrays [78]. Each single printed Yagi-Uda array was designed with a driven dipole, 18 directors, and one reflector, each printed on both sides of a 0.127 mm thick RT/Duroid 5880 substrate ($\varepsilon_r = 2.2$). There therefore is no ground plane in the antenna's structure. One half of each driven dipole is placed on either side of the dielectric substrate. Symmetrical parallel lines are used as a feeding structure, printed on both sides of the substrate.

The polarization of this antenna is parallel to the substrate. A 10 dB impedance bandwidth, from 55 GHz to 60 GHz, was achieved. The measured gain was 15 dBi at 60 GHz. The 3 dB beamwidths of this antenna in free space were 29° and 19° in the H and E planes, respectively.

Another type of Yagi-Uda antenna was proposed for on-body communications at 60 GHz (Figure 13 [79]). A substrate-integrated waveguide (SIW) structure was placed on the left side of the antenna; two periodic rows of metallic vias formed the waveguide sidewalls. The substrate used here was RT/Duroid 5880 substrate ($\varepsilon_r = 2.2$), with a thickness of 0.787 mm.

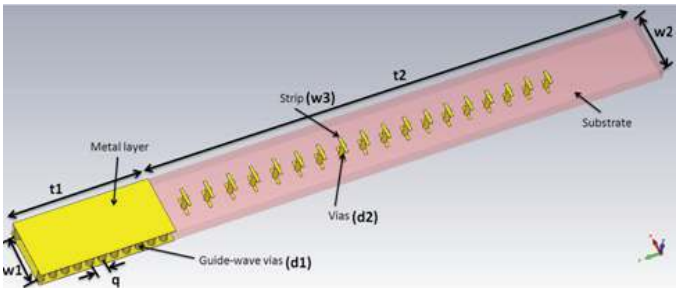

Figure 13. A schematic drawing of the SIW Yagi-Uda antenna (reproduced from [80]).

The width of the substrate-integrated waveguide was $w_1 = 2.6$ mm. The diameter and spacing of the vias were $d_1 = 0.4$ mm and $q = 0.65$ mm, respectively. Another row of vias with a diameter of $d_2 = 0.3$ mm was also inserted into the substrate to act as directors. The vias were loaded at the top and bottom with printed strips to make sure that the equivalent length of the directors was a half-wavelength. As high currents flowed in the vias of the parasitic elements, the radiated polarization was normal to the substrate, unlike the printed Yagi array described earlier, which was horizontally polarized. The measured gains without and with the phantom were 12.5 dBi and 10 dBi, respectively. The 3 dB beamwidths of this antenna in free space were 26° and 25° in the H and E planes, respectively.

Antenna measurements with a body-tissue phantom and a real human body were done to investigate the performance of both antennas in close proximity to the human body [80]. Note that there was no ground plane between the antenna and the phantom. Figure 14 shows the co-polarized radiation pattern of the printed Yagi-Uda array in proximity to a phantom. The solid and dashed curves show the radiation patterns measured in free space and simulated in close proximity to a numerical skin phantom, respectively. The dotted curve and the dash-dotted curves represent the radiation patterns measured in close proximity to the fresh meat and the physical skin phantom [64], respectively. The measured maximum gains obtained with the phantom in the H and E planes were around 18 dBi and 15 dBi, respectively. Due to the presence of the phantom, the main beam of the radiation pattern in the H plane was lifted upwards away from the phantom by about 12°. In the E plane, all normalized radiation patterns showed good agreement.

Although different types of phantoms were used, the results showed good agreement with each other. However, due to the smaller size of the numerical phantom used in the simulation, the beamwidth of the simulated pattern was wider and the shift of the maximum gain direction was smaller.

5.3 Microstrip Patch Array for Off-Body Communications

Patch antennas are simple, low-profile, light weight, and low-cost structures, and their broadside radiation allows improving the power-budget link and reducing radiation towards the body. For these reasons, patch antennas are very attractive solutions for off-body communications.

A microstrip-fed four-patch single-layer antenna array (Figure 15), printed on a thin RT Duroid 5880 substrate ($h = 127$ µm, $\varepsilon_r = 2.2$, $\tan\delta = 0.003$) was proposed in [81]. A 2×2 antenna array allowed reaching a gain of 12 dBi with about the same beamwidth in the E and H planes. The antenna's performance was investigated with and without a phantom. The simulated and measured radiation patterns, obtained both in free space and with a skin-equivalent phantom, are shown in Figure 16. The measured gain, directivity, and efficiency in free space and on the skin-equivalent phantom are summarized in Table 5. Compared to end-fire radiating antennas, the effects of the phantom on the broadside-radiating antennas was much less pronounced, and the antenna performance was nearly insensitive to the presence of a phantom. This was due to the antenna essentially radiating in a direction opposite to the phantom, and the radiating element being shielded from the body by a ground plane.

5.4 Textile Antenna at 60 GHz

Textile antennas have been extensively studied over the last few years since they guarantee flexibility and can be

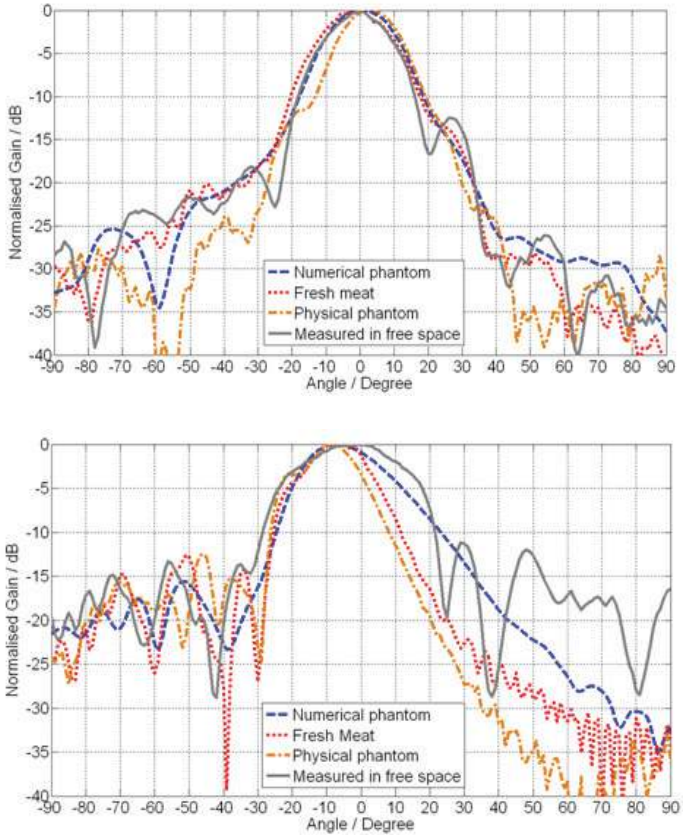

Figure 14. The radiation patterns of the printed Yagi-Uda array in close proximity to the phantom: (a, top) the E plane (*xy*); (b, bottom) the H plane (*xz*).

Figure 15. The antenna array mounted on a cylindrical skin-equivalent phantom (the total antenna size without connector was 8 mm × 20 mm).

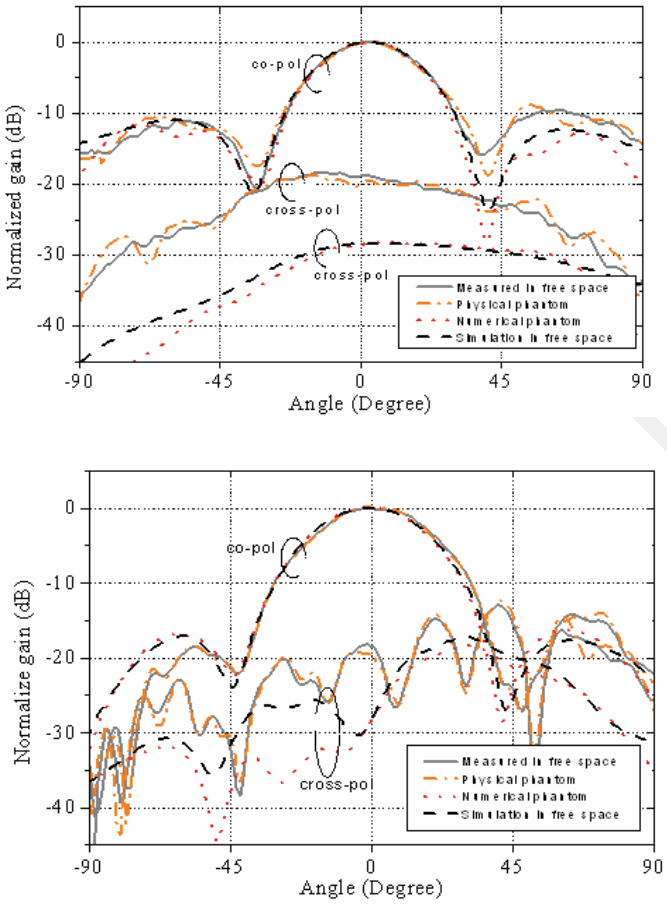

Figure 16. The measured and simulated radiation patterns at 60 GHz in the E (a, top) and H (b, bottom) planes.

Table 5 Measured gains, directivities, and efficiencies.

	Gain [dBi]	Directivity [dBi]	Efficiency [%]
In free space	11.8±0.3	13.9±0.3	62
Physical phantom	11.9±0.3	14.1±0.3	60

directly integrated into clothing. Developing millimeter-wave textile antennas is a technological challenge, since high fabrication accuracy is required. Moreover, to facilitate the commercialization of textile antennas, the choice of the substrate should be limited to commonly used fabrics. For millimeter waves, the textile substrate should be properly selected and characterized, as its thickness, permittivity, and loss tangent are of great importance to designing high-efficiency antennas with satisfactory performance. Recently, it was demonstrated that commercial textiles can be used as antenna substrates at 60 GHz [82, 83].

A reproducible and accurate on-textile fabrication process was developed, and a microstrip-fed four-patch single-layer antenna array, printed on a 0.2 mm-thick textile, was proposed [83] (Figure 17). A dimensional tolerance of the order of 10 μm was reported. Several prototypes were fabricated and measured in reflection and radiation under various conditions. The simulated and measured antenna efficiencies were 45% and 41%, respectively. However, high losses were due to the presence of the 15.2 mm-long feed line (i.e., 3.3 dB), employed to avoid unwanted reflections from the V connector. In order to increase the antenna's gain and efficiency, the feed line could be shortened or even suppressed (e. g., by excitation of the array at its center). In this last case (no feed line), a 12.6 dBi gain and 75% efficiency could be achieved, according to the numerical estimations. In addition, comparison between measurements in free space and on a skin-equivalent phantom showed that the human body has a very weak impact on the antenna's performance. This can be explained by the presence of an electrically large ground plane.

Furthermore, the influence of bending was investigated numerically and experimentally. It was demonstrated [83] that bending had a small impact on the reflection coefficient and antenna gain.

A microstrip-fed Yagi-Uda textile antenna (Figure 18) was proposed in [82]. The structure was made of a driven dipole and 10 directors, printed on the top layer of a textile substrate (here, a 0.2 mm-thick fabric obtained from a cotton shirt). In the presence of a phantom, the reflection coefficient was slightly affected, as illustrated in Figure 19. Different antenna-to-phantom spacings were considered, as they may fluctuate in practice, due to body movements. Figure 20 presents the simulated radiation pattern for different spacings, *d*, demonstrating that the maximum gain, the gain at broadside, and the tilt angle decreased with *d*.

5.5 Woodpile EBG-Based Antennas

As discussed above, antennas that exhibit an omnidirectional pattern in the plane parallel to the body and a narrow beam in the orthogonal plane are suitable for use in on-body communications. Indeed, such antennas reduce losses due to the off-body transmissions, confining the energy in proximity

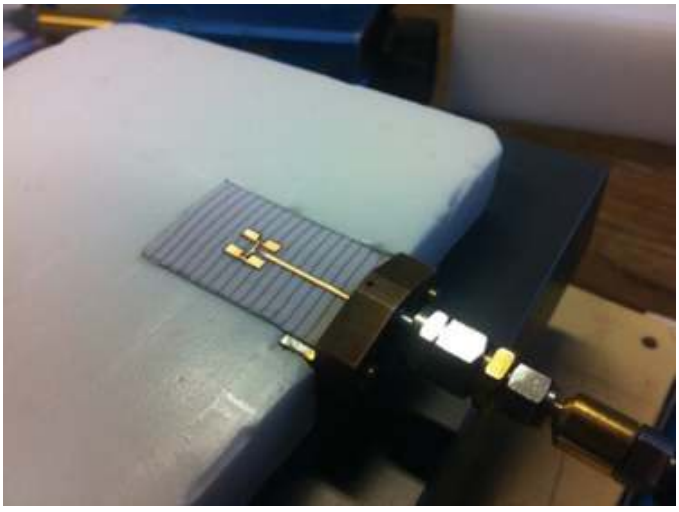

Figure 17. The textile antenna array mounted on a parallelepiped skin-equivalent phantom.

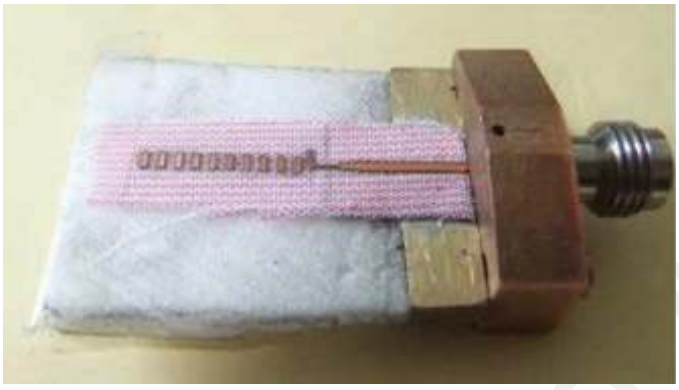

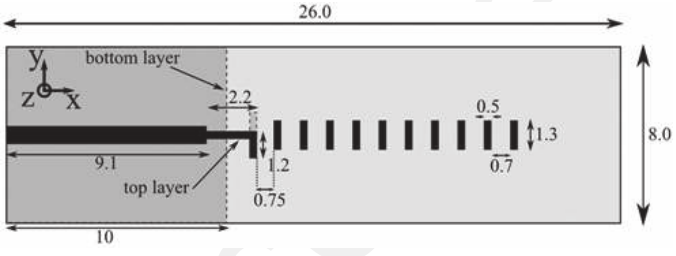

Figure 18. The antenna design: (a, top) the antenna prototype placed on a foam support and fed by a V connector for measurement purposes; (b) the antenna geometry and dimensions (mm) (reproduced from [82]).

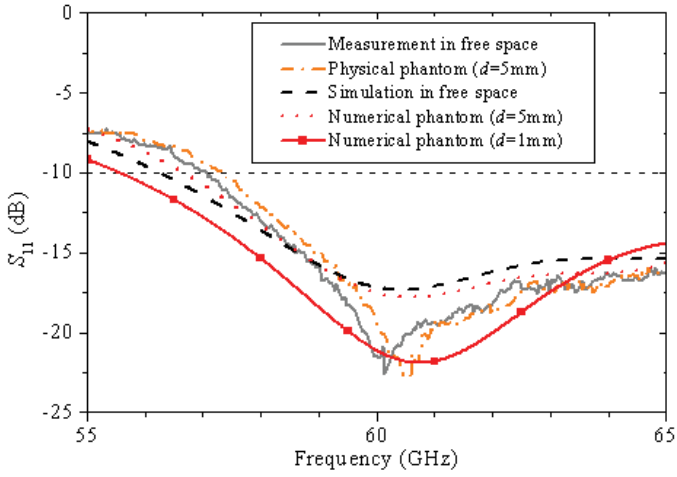

Figure 19. The simulated and measured reflection coefficients of the textile antenna for different antenna/body distances, *d*.

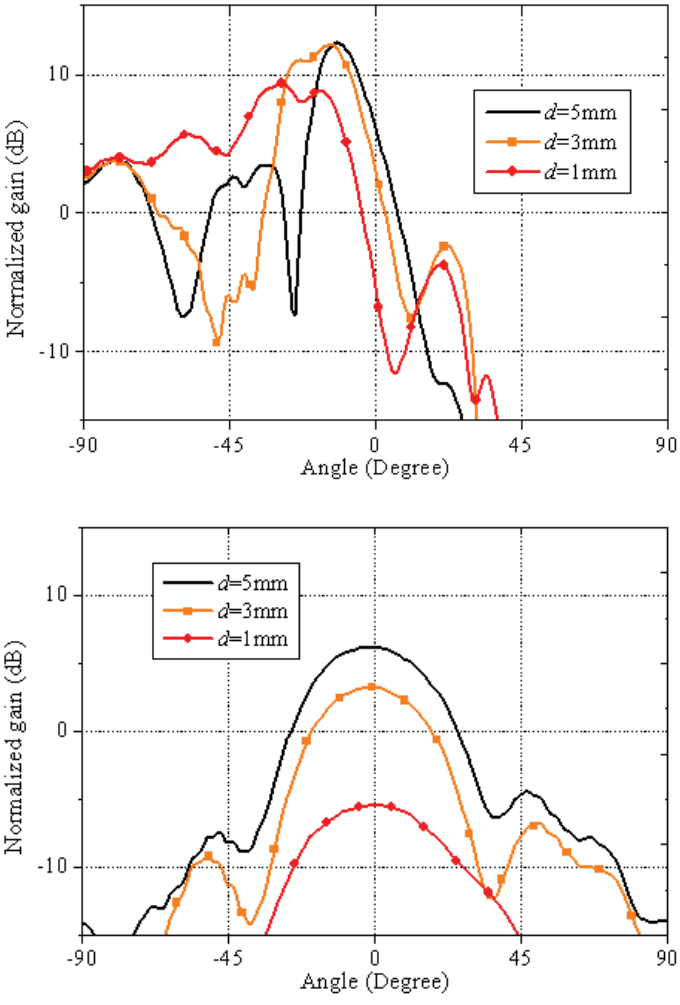

Figure 20. The simulated co-polarization components on the phantom at 60 GHz for three different antenna/body separations, *d*: (a, top) H plane, (b, bottom) E plane.

to the human body. On the other hand, antennas that exhibit high directivity in the plane orthogonal to the human body are suitable for body-to-body and off-body communications. In order to improve the directivity without resorting to arrays, reflectors, or lenses, the concept of a partially reflecting resonator, introduced by Trentini [84], was used. The original design of a woodpile antenna, operating at 94 GHz, was proposed in [85]. In particular, both a flat and a cylindrical antenna were designed for on-body communications and off-body communications, respectively. The unit cell and the periodic structure of the woodpile EBG resonator used for the planar and the cylindrical antenna are shown in Figure 21.

The planar woodpile structure consisted of stacked diffraction gratings, in which adjacent layers were perpendicular to each other (Figure 21a). The dimensions of the unit cell were $l = 1.67$ mm and $d = 0.41$ mm. This structure possessed face-centered tetragonal symmetry, and provided a full three-dimensional bandgap. The unit cell of the cylindrical woodpile (Figure 21b) differed from the planar woodpile in the form of stacking perpendicular filaments that were not interleaved. In this case, the dimensions of the unit cell were $l = 1.23$ mm and $d = 0.41$ mm. Although the new structure did not exhibit a full three-dimensional bandgap, the cavity was excited by an electric field polarized along the axis of the cylinder. Three-dimensional microwave periodic structures can be realized using conventional machining techniques that however are not suited for millimeter-wave frequencies, as the dimensions of the geometries are small, typically of the order of fractions of a millimeter. More-sophisticated techniques, such as silicon lithography, are available, but they are better suited for terahertz and optical wavelengths. In this case, the woodpile structure can be produced by using a rapid and cost-effective extrusion free-forming technique, as presented in [86].

The design of the two antennas has been extended in order to change the operating frequency at 60 GHz [77, 87, 88]. By referring to Figure 21, the unit cell of the planar structure exhibited $l = 2.17$ mm and $d = 0.54$ mm, while $l = 1.8$ mm and $d = 0.6$ mm for the cylindrical structure.

Figure 22 shows the planar resonant antenna, which consisted of a WR15 waveguide, the woodpile structure, and a ground plane. By using the woodpile, the maximum directivity was increased more than 10 dB compared to the open waveguide. This antenna was proposed for off-body communications.

The cylindrical-resonator antenna was proposed for on-body communications, as shown in Figure 23. A woodpile cylindrical resonant cavity is applied to the monopole-like feeder, which exhibited the following dimensions: $h_d = 2.1$

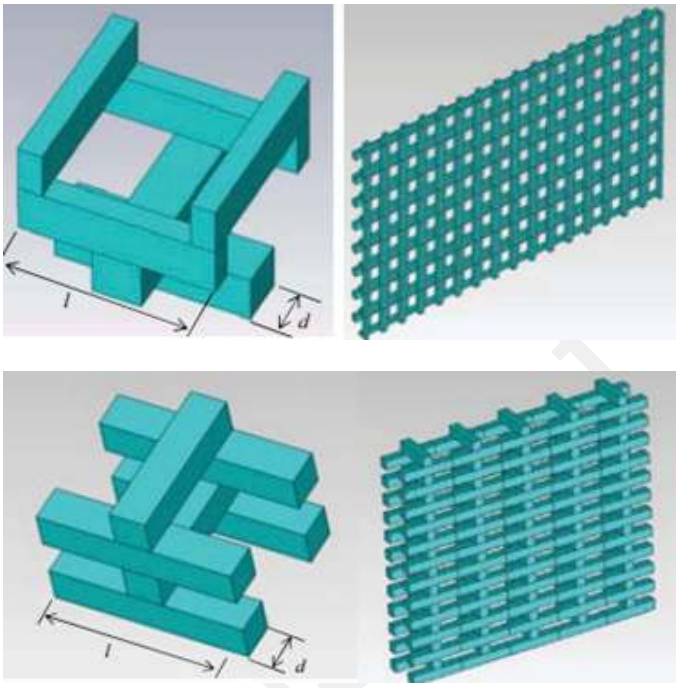

Figure 21. Woodpile EBG structures: (a, top) the unit cell and periodic structure for the planar woodpile; (b) the unit cell and periodic structure for the cylindrical woodpile (reproduced from [77]).

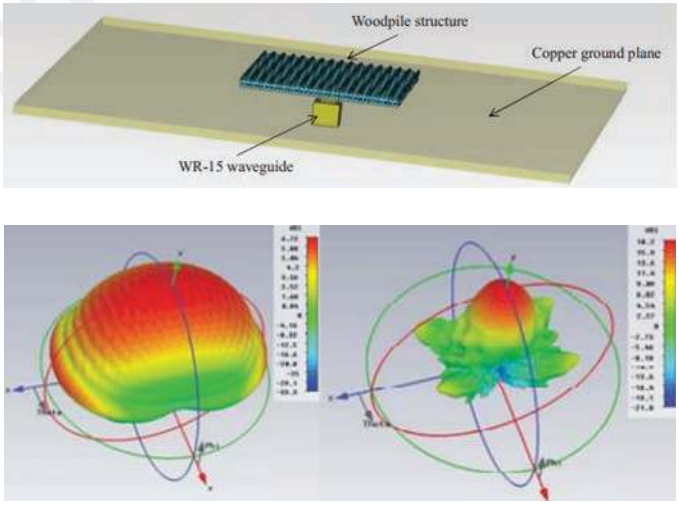

Figure 22. The planar resonant antenna: (a, top) the antenna's structure; (b, bottom) the radiation pattern at 60 GHz for the waveguide (left), and for the planar resonant antenna (right) (reproduced from [77]).

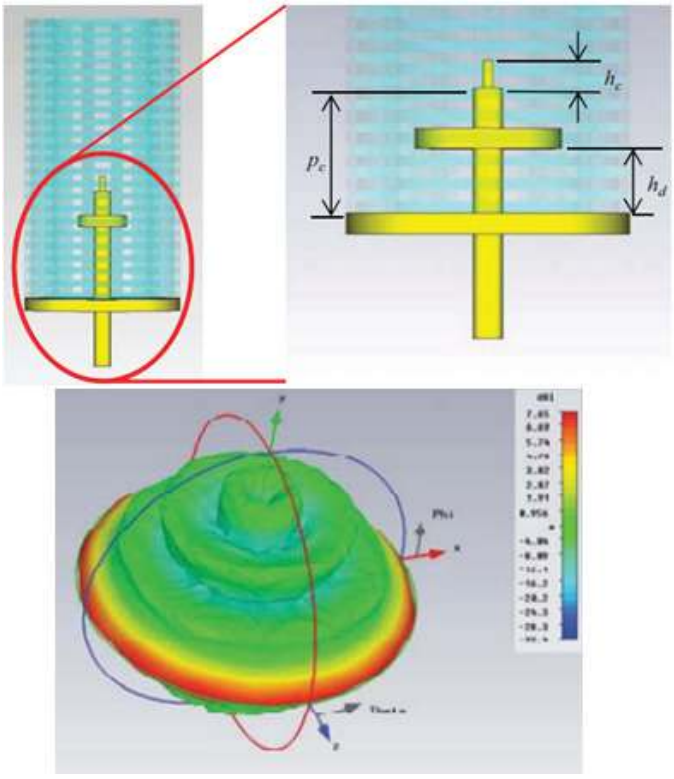

Figure 23. The cylindrical resonator antenna and its radiation pattern (reproduced from [77]).

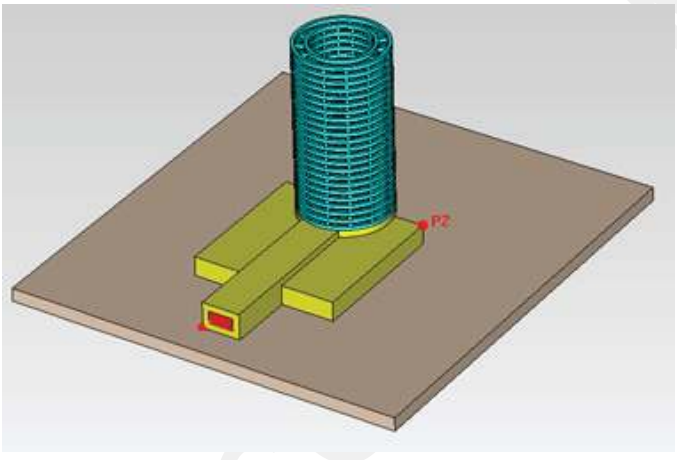

Figure 24. The antenna over a dry-skin digital phantom.

mm, $p_c = 9.5$ mm, and $h_c = 1.3$ mm. The maximum directivity was improved by more than 5 dB compared to a conventional monopole antenna.

The performance of the antenna placed close to the human body was investigated. This operating environment can have a potentially disruptive effect on the free-space antenna's characteristics. To this aim, the antenna was simulated in proximity to a 60 mm × 60 mm digital phantom, having the electrical properties of skin at 58 GHz (Figure 24). The in situ radiation pattern obtained is shown in Figure 25. It could be readily seen that it was similar to that for free space, and retained the maximum directivity in the plane parallel to the surface of the phantom. This was due to the limited radiation along the axis of the cylinder, which reduced the interaction with the underlying tissues. A prototype of the cylindrical antenna was fabricated, and is shown in Figure 26.

5.6 Reconfigurable Antenna

A reconfigurable antenna is useful in minimizing unwanted illumination of the wider body area whilst overcoming the fading or shadowing resulting in the loss of line-of-sight paths by switching its radiation pattern's beam direction. This strategy also leads to higher security, as the energy can be confined to the immediate vicinity of the body, thus giving good body-to-body and on-body-to-off-body receiver isolation. If and when required, such on-body antennas can switch to an outward-facing beam. This has long been an aspiration for microwave on-body communications; however, the low directivity of small antennas prevents them from being practically realized at lower frequencies (e.g., at 2.4 GHz). Nevertheless, this idea can be realized at 60 GHz because of the small size of the antennas and the wide available bandwidth. Due to the wideband unlicensed spectrum around 60 GHz, the frequency-scanning technique is the easiest way to implement the pattern reconfigurability for propagation-channel measurements. Although implementing this approach in on-body communications may require more signal processing and add to the system complexity, it can still be beneficial in some special cases, where beam reconfigurability is required only on one side of the link and a fixed-beam wideband antenna can be used on the other side, so that the frequency of operation can be varied in order to steer the beam as required by the channel conditions.

A substrate integrated-waveguide frequency-scanning antenna was proposed for this application (Figure 27). There were multiple slot pairs on the top metal layer of the substrate-

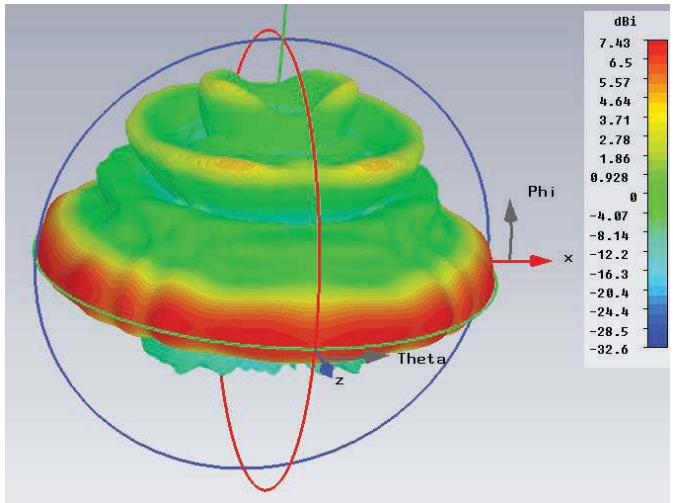

Figure 25. The radiation pattern on a dry-skin digital phantom (reproduced from [88]).

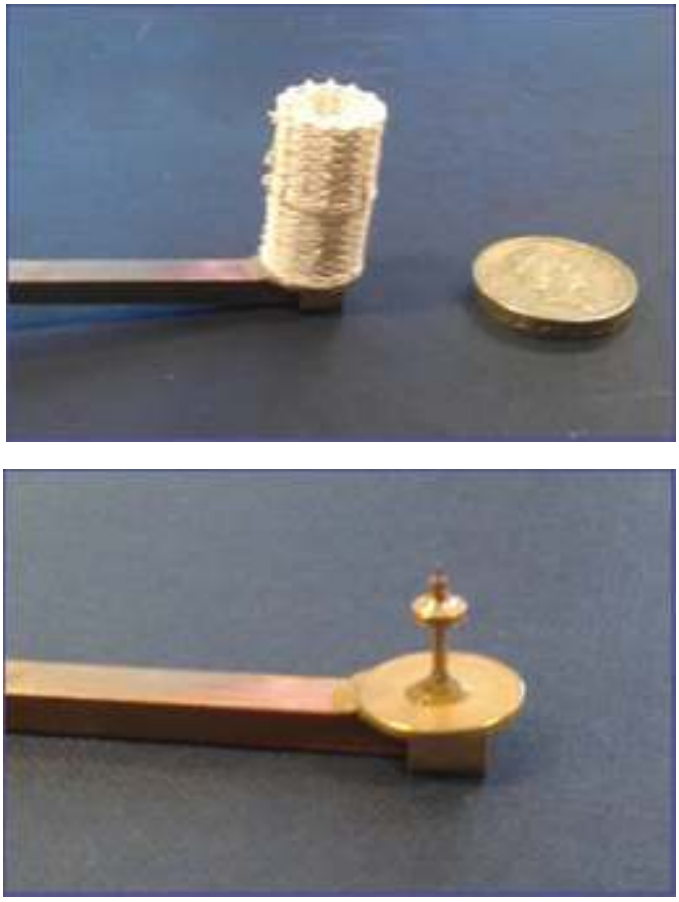

Figure 26. The fabricated prototype: (a, top) the complete antenna, and (b, bottom) the feeding structure.

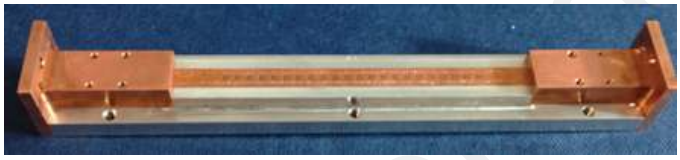

Figure 27. The prototype of the substrate-integrated waveguide-slot antenna.

integrated waveguide. Quarter-guided-wavelength-spaced slot pairs introduced reflection cancellation to improve the realized gain. This also achieved a wide impedance bandwidth, from 57 GHz to 64 GHz. Since this was a traveling-wave antenna, higher power was consumed compared to resonant antennas. By scanning the frequency, the main beam of the radiation pattern was accordingly scanned. The coverage angle was from $-30°$ to $30°$ for both ports, but with a null at the center ($0°$). The measured radiation pattern is shown in Figure 28 when one port was excited. The gain of antenna was approximately 15 dBi.

For the considered frequencies, the power absorption in the body was superficial, and the dosimetric techniques available at lower microwave frequencies could not be used at millimeter waves. A multi-physics dosimetric approach was recently implemented at 60 GHz to investigate the specific absorption rate (SAR), incident power density (IPD), and power density (PD) in the phantom. These characteristics were retrieved from the superficial temperature dynamics recorded using a high-resolution infrared camera [81].

As an application example, the local peak SAR and incident power density distributions were simulated and experimentally determined for the microstrip patch antenna array (see Section 5.3) placed 5.6 mm above the phantom [81]. The experimental and numerical results were in very good agreement (Figure 29). It was also demonstrated that for the considered scenario, even the relatively high input power of the antenna (up to 550 mW for an antenna/body separation of 1 mm) resulted in exposure levels that were below international exposure guidelines (i.e., 20 mw/cm^2 averaged over 1 cm^2). It is worthwhile to underline that in practice, the antenna's input power is expected to be restricted to several tens of mW to comply with the regulations (see Table 1), and to reduce the power consumption of battery-powered sensors. This dosimetric technique can be also used for the determination on the on-phantom antenna efficiency [89].

Bioelectromagnetic issues related to the exposure of users are out of the scope of this paper. They were studied elsewhere (e.g., [90-92]), and have recently been reviewed in a separate paper [9].

6. Propagation Channel Characterization

Path-loss characterization is a fundamental step in the analysis of the on-body propagation channel. A review of some recent studies performed for different links of interest is presented in the next sections.

6.1 Head-to-Shoulder Link

The head-shoulder link was investigated in [33, 34], using a ray-based technique. In particular, a numerical model

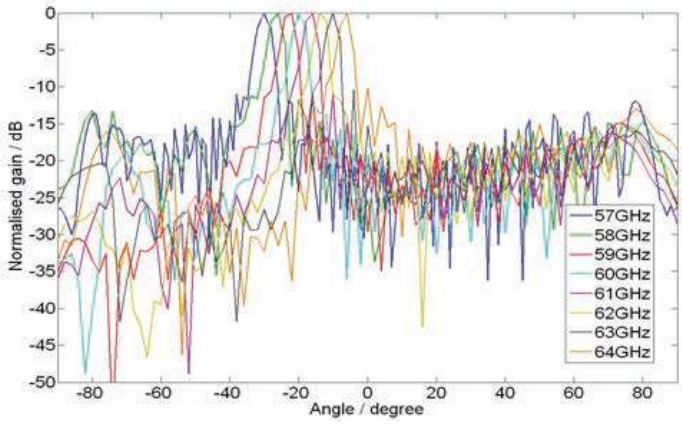

Figure 28. The radiation pattern for the substrate-integrated waveguide-slot antenna.

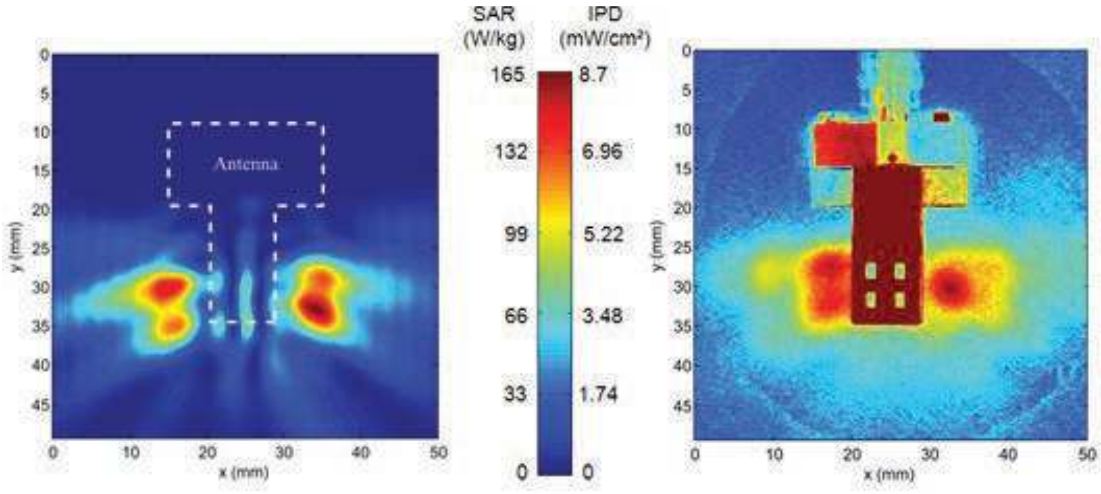

Figure 29. The SAR and incident power-density distributions at 60 GHz for a microstrip off-body antenna array (the input power was 322 mW). The numerical results for the antenna on the skin are shown on the left, and the measurements on the skin-equivalent phantom are shown on the right. Most of the absorption occurred in the E plane of the antenna.

composed of facets was considered, and the dielectric properties of dry skin were assigned to the model. The transmitter antenna was fixed on the head of the subject, above the left ear. The receiver was placed near the left shoulder, at a range of several distances from the transmitter. The radiation pattern of the flanged rectangular waveguides, operating at 94 GHz and measured in free space, was assigned to the antennas. A comparison between the simulated link (Figure 30a) and the measurements (Figure 30b), carried out on a human subject, is shown in Table 6.

The same link was investigated at a frequency of 60 GHz by using a parallel implementation of the FDTD method [93]. The investigated case represented a limiting case where a ray-based technique was suitable for such large problems, and a full-wave technique, such as the FDTD, was still not computationally inefficient. Table 7 shows a comparison of path-loss values obtained for the head-to-shoulder link by using a ray-based technique and the FDTD method.

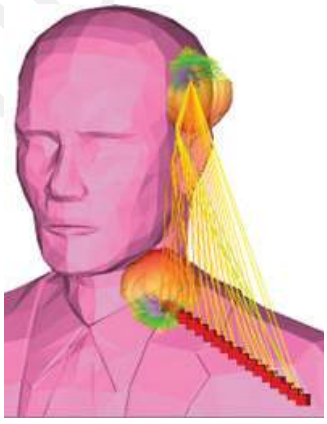

Figure 30. The head-to-shoulder link: the numerical simulation (reproduced from [33]) (a, top) and the measurement setup (b, bottom).

6.2 Waist-to-Trunk Link

A study of the waist-trunk link was proposed in [33] and [35]. A digital phantom was considered for this investigation. The electromagnetic properties of the clothes were assigned as described in [35]. The transmitter was placed on the left side of the belt, and the receiver position was varied over a grid of different positions at the front of the subject's trunk. The measured free-space radiation pattern of the WR10 open-ended waveguide was assigned to the antennas. The measurement setup was chosen in order to replicate the simulated setup (Figure 31).

The path-loss distribution obtained as a function of the normalized distance between the transmitter and receiver was

Table 6. A comparison among simulated and measured data for the head-to-shoulder link at 94 GHz [34].

Tx-Rx Distance [cm]	Measured Free Space Path Loss [dB]	Measured On-Body Path Loss [dB]	Simulated Path Loss [dB]
23.4	45	44.5	41.5
28.7	47	47.5	49.3
29.5	48	51	50.6

Table 7. A comparison of the path loss in terms of the path-loss exponent model for simulated and measured data at 94 GHz.

Tx-Rx Distance [cm]	FDTD Simulation [dB]	Ray Tracing Simulation [dB]
13.6	50.1	51.0
15.7	50.2	51.5
17.3	51.1	52.1
19.5	51.6	51.6

Table 8. A comparison of the path loss in terms of the path-loss exponent model for simulated and measured data at 94 GHz.

Data Set	Path Loss Exponent	σ [dB]
Simulated [35]	3.87	13.6
Simulated [33]	3.79	17.8
Measured	4.36	6.4

Table 9. The measured path gain [dB] for the wrist-chest channel.

Arm Position	Slot Antenna	Horn	Monopole
40°	–43	×	×
30°	–43.4	×	–60.7
20°	–41.3	–59.7	–51.4
10°	–32.9	–45.1	–43.7
0°	–50.8	–50.8	–56.8
–10°	–45.8	–50	–51.2
–20°	–51.8	–57.9	–54.2
–30°	–53.2	–58.3	–63.9
–40°	–52	×	×

× signal below noise level

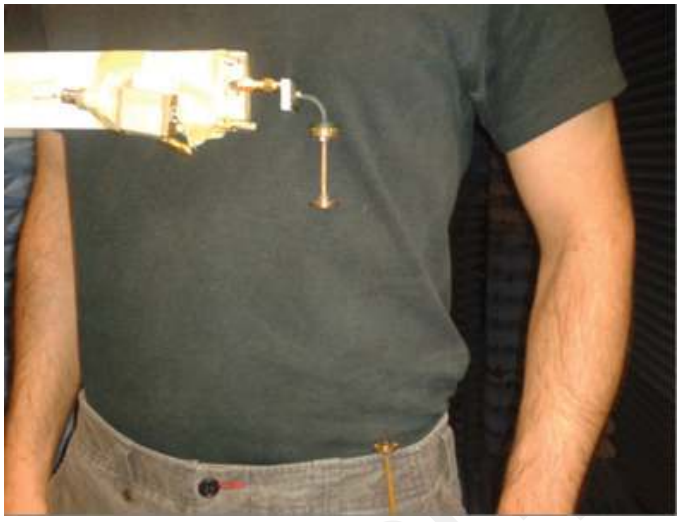

Figure 31. The measurement setup for the waist-to-trunk link.

Figure 32. The antenna placements for the wrist-chest channel measurement and body posture (40°).

compared with the measured distribution. In particular, a linear-regression fit for the path-loss distance dependence was calculated according to the conventional path-loss-exponent model. Table 8 shows a comparison of the path-loss exponent and shadowing factor, σ, obtained from measurements and simulations.

6.3 Wrist-to-Chest Link

On-body channel measurements were conducted for a wrist-to-chest link in order to test the hypothesis that employing a reconfigurable antenna could improve the performance by using beam scanning. As shown in Figure 32, a wideband horn antenna, covering frequencies from 57 GHz to 64 GHz, was placed on the wrist, facing upwards, and the slot antenna was placed on the chest, facing downwards. The horn was used as the transmitting antenna, and the signals received by both ports of the slot antenna were simultaneously monitored. In the measurement, the subject was swinging its arm sideways, from

right to left. However, as the vector network analyzer took a long time to sweep the frequency range from 57 GHz to 64 GHz, it proved to be not fast enough to capture the motion. The subject therefore had to keep still during each frequency sweep. Hence, nine static postures were adopted during this arm-swing motion. The arm-lift angle was varied from approximately 40° to –40° in steps of 10°. In order to make meaningful comparisons, the measurement was repeated by replacing the reconfigurable slot antenna with a horn antenna, and subsequently with a monopole antenna.

The measured results are shown in Table 7. These results demonstrated that the frequency-scanning antenna achieved the pattern reconfigurability in principle (the control loop that achieved this in practice had to be implemented), and could improve the link's performance.

6.4 Analytical, Numerical, and Experimental Study on a Flat Phantom

On-body propagation at 60 GHz was studied analytically, numerically, and experimentally using a flat skin-equivalent phantom in [89].

First, to provide a fundamental theoretical model of the path gain, the propagation along a planar homogeneous skin-equivalent phantom was studied analytically by considering vertical and horizontal elementary dipoles. For a vertically-polarized wave and for a distances from several cm up to 20 cm ($40\lambda_0$), the path-gain model depended on the height, *h*, of the dipole above the phantom. If $h > 3$ mm, the power-decay exponent $n = 4$. If $h < 3$ mm, the path gain could be modeled similarly to the path gain at lower microwave frequencies, i.e., $n = 3.5$. Moreover, since the electrical size of the body at 60 GHz was much larger than at microwaves, a new region, corresponding to the distances beyond $40\lambda_0$ (20 cm) was of practical interest at 60 GHz: for this region, $n = 4$. For a horizontally-polarized wave, a power-decay exponent of $n = 4$ was found for the whole range of distances.

Second, propagation along the body was investigated experimentally in the vertical and horizontal polarizations using two linearly-polarized open-ended waveguides. The experimental results were in good agreement with analytical models and full-wave simulations, thereby showing that the on-body propagation could be accurately represented by the analytical path-gain model.

It is interesting to note that the path gain was highly sensitive to the antenna/body separation, *h*. It increased with *h*, and became even higher than the free-space value for H polarization at $h = 5$ mm.

7. Conclusion

An overview of the challenges and progress in modeling body-centric scenarios at millimeter-wave frequencies has been presented in this paper. First, the worldwide regulations for V and W bands were introduced, with a focus on the North American and European circumstances. The frequency bands available in each country for commercial use were listed, distinguishing between licensed and unlicensed allocations. Subsequently, the numerical methodologies for investigating on-body propagation were presented, with particular attention to advantages and challenges presented by each technique. Ray-based techniques allow analyzing electrically large structures without incurring a high computational burden. On the other hand, the accuracy of the results is strongly dependant on the accuracy of the scenario, and on the antenna's positioning. Classical techniques, such as FDTD and the MoM, were revealed to be appropriate methodologies, as well. However, although these methods provide accurate results, they can be efficiently used to analyze a limited portion of the human body.

Recent progress in the manufacturing and availability of both experimental and numerical phantoms has been outlined. The accuracy of these phantoms plays a key role in the proper understanding of both propagation phenomena and actual in situ antenna performance on the human body. Accurate numerical models (surface or volumetric) can be obtained by means of advanced imaging techniques, and can make simulations a very powerful tool for on-body radio-channel characterization. Measurements are also widely used to investigate the propagation around the human body. However, such measurement are scarcely reproducible, and are limited by the safety of the subject. In order to overcome these issues, experimental phantoms that have the shape of parts of the human body and present the electromagnetic properties of human tissues have been implemented. So far, semisolid phantoms are the most commonly used. Mixtures of water and other agents allow representing electromagnetic properties of human tissues at millimeter-wave frequencies, although the applicability range is limited at present between 55 GHz and 65 GHz.

Concerning antenna design, an overview of the available technologies in terms of wearable antennas, resonator antennas, patch antennas, and reconfigurable antennas has been provided and discussed. For some of these, the performance obtained when the antenna is placed in close proximity to the human body has been evaluated.

Finally, the characterization of the propagation channel has been provided for different links, such as head-to-shoulder, waist-to-trunk, and wrist-to-chest. The aims of these analyses were not only to prove the agreement between simulations and measurements and to evaluate link performance, but also to provide a complete view for understanding body-centric propagation at millimeter-wave frequencies.

8. Acknowledgment

The authors thank EPSRC for providing the funding for this research activity, under Grants EP/I009019/1 and EP/I010491/1. This work was supported by "Agence Nationale de la Recherche" (ANR), France under Grants ANR-09-RPDOC-003-01 (Bio-CEM project), by Labex CominLabs and Brittany Region under ResCor/BoWi project, and by "Centre National de la Recherche Scientifique (CNRS)," France. In addition, the authors thank Dr. Xuesong Lu and Prof. Julian R. G. Evans for fabricating the woodpile antenna, Dr. Akram Alomany and Prof. Clive Parini for the useful discussions, and Prof. John Batchelor, University of Kent, for his precious advice.

9. References

1. T. Yilmaz, R. Foster and Y. Hao "Detecting Vital Signs with Wearable Wireless Sensors," *Sensors 2010*, **10,** 12, 2010, pp. 10837-10862.

2. Y. Hao and R. Foster, "Wireless Body Sensor Networks for Health-Monitoring Applications," *Physiological Measurement*, **29**, 11, 2008, pp. R27-R56.

3. C. Otto, A. Milenkovic, C. Sanders and E. Jovanov, "System Architecture for a Wireless Body Area Network for Ubiquitous Healthcare Monitoring," *Journal of Mobile Multimedia*, **1**, 4, 2006, pp. 307-326.

4. M. Patel and J. Wang, "Applications, Challenges, and Prospective in Emerging Body Area Networking Technologies," *IEEE Wireless Communications*, **17**, 1, 2010, pp. 80-88.

5. Future Soldier, http://en.wikipedia.org/wiki/Future_Soldier.

6. Selex Sistemi Integrati, "Forza NEC" project, http://www.selex-si.com/IT/Common/files/SelexSI/brochure_datasheet/2008/Brochure/forzanec_ITA_low.pdf

7. Nike+ http://nikeplus.nike.com/plus/.

8. S. L. Cotton, W. G. Scanlon and B. K. Madahar, "Millimeter-Wave Soldier-to-Soldier Communications for Covert Battlefield Operations," *IEEE Communications Magazine*, **47**, 10, October 2009, pp. 72-81.

9. M. Zhadobov, N. Chahat, R. Sauleau, C. Le Quement and Y. Le Dréan, "Millimeter-Wave Interactions with the Human Body: State of Knowledge and Recent Advances," *International Journal of Microwave And Wireless Technologies*, **3**, 2, April 2011, pp. 237-247.

10. P. Adhikari, "Understanding Millimeter Wave Wireless Communication," Loea Corporation, 2008.

11. Report and Order of the Federal Communications Commission, FCC 03-248, November 2003.

12. Public Notice of the Federal Communications Commission, DA 05-311, February 2005.

13. Federal Communications Commission, Code of Federal Regulation, Title 47 Telecommunication, Chapter 1, part 15.255, October 2004.

14. Federal Communication Commission, Code of Federal Regulation, Title 47 Telecommunication, Chapter 1, part 101, October 2004.

15. S. K. Su Yong and C.-C. Chong, "An Overview of Multi-Gigabit Wireless through Millimeterwave Technology: Potentials and Technical Challenges," *EURASIP Journal on Wireless Communications and Networking*, **2007**, 2007.

16. P. S. Hall and Y. Hao, *Antennas and Propagation for Body-Centric Wireless Communications*, Norwood, MA, Artech House, 2006, pp 271-274.

17. Spectrum Management and Telecommunications, Radio Standard Specification-210, Issue 6, Low-Power Licensed-Exempt Radio Communication Devices (All Frequency Bands), Category 1 Equipment, September 2005.

18. Japan Regulations for Enforcement of the Radio Law 6-4-2, Specified Low Power Radio Station (11) 59-66 GHz Band.

19. European Telecommunications Standard Institute DTR/ERM-RM-049, "Electromagnetic Compatibility and Radio Spectrum Matters (ERM), System Reference Document, Technical Characteristics of Multiple Gigabit Wireless Systems in the 60 GHz Range," March 2006.

20. Australian Communications and Media Authority, "Radiocommunications (Low Interference Potential Devices) Class License Variation 2005 (no. 1)," August 2005.

21. Ministry of Information and Communication of South Korea, "Frequency Allocation Comment of 60 GHz Band," April 2006.

22. ECC Recommendation (05)07, "Radio Frequency Channel Arrangements for Fixed Service Systems Operating in the Bands 71-76 GHz and 81 - 86 GHz," Revised Dublin 2009

23. AMS Technologies, http://www.amstechnologies.com/.

24. Ceragon Networks, http://www.ceragon.com/.

25. Bridgewave Communications, http://www.bridgewave.com/.

26. T. S. Rappaport, *Wireless Communications: Principles and Practice*, New York, Prentice Hall, 2001.

27. J. B. Keller, "Geometrical Theory of Diffraction," *Journal of the Optical Society of America*, **52**, 2, 1962, pp. 116-130.

28. J. D. Parsons, *The Mobile Radio Propagation Channel*, Chichester, John Wiley and Sons, 2000.

29. G. Tiberi et al., "Analysis of Realistic Ultra-Wideband Indoor Communication Channels by Using an Efficient Ray-Tracing Based Method," *IEEE Transactions on Antennas and Propagation*, **APS-57**, 3, March 2009, pp. 777-785.

30. M. Ghaddar, L. Talbi, T. Denidni and A. Sebak, "A Conducting Cylinder for Modeling Human Body Presence in Indoor Propagation Channel," *IEEE Transactions on Antennas and Propagation*, **AP-55**, 11, 2007, pp. 3099-3103.

31. S. Collonge, G. Zaharia and G. El Zein, "Influence of the Human Activity on Wide-Band Characteristics of the 60 GHz Indoor Radio Channel," *IEEE Transactions on Wireless Communications*, **3**, 6, November 2004, pp. 2396-2406.

32. S. Alipour, F. Parvaresh, H. Gajari and D. F. Kimball, "Propagation Characteristics for a 60 GHz Wireless Body Area Network (WBAN)," Military Communications Conference, San Jose, 2010.

33. A. Pellegrini, A. Brizzi, L. Zhang and Y. Hao, "Numerical and Experimental Analysis of the On-Body Propagation Channel at W Band," European Conference on Antennas and Propagation, Prague, 2012.

34. P. Usai, A. Monorchio, A. Brizzi, A. Pellegrini, L. Zhang and Y. Hao, "Analysis of On-Body Propagation at W Band by Using Ray Tracing Model and Measurements," IEEE International Symposium on Antennas and Propagation, Chicago, 2012.

35. A. Pellegrini, A. Brizzi, L. Zhang and Y. Hao, "Path Loss Characterization in Body-Centric Scenario at 94GHz," *IEICE Transactions on Communications*, **E96-B**, 10, October 2013 (to appear).

36. K. S. Yee, "Numerical Solution of Initial Boundary Value Problems Involving Maxwell's Equations in Isotropic Media," *IEEE Transactions on Antennas and Propagation*, **AP-14**, 3, 1966, pp. 302-307.

37. P. S. Hall and Y. Hao and S. L. Cotton, "Progress in Antennas and Propagation for Body Area Networks," International Symposium on Signal Systems and Electronics, Nanjing, 2010.

38. P. S. Hall and Y. Hao, *Antennas and Propagation for Body-Centric Wireless Communications*, Norwood, MA, Artech House, 2006.

39. Q. H. Abbasi, A. Sani, A. Alomainy and Y. Hao, "Numerical Characterization And Modeling Of Subject-Specific Ultrawideband Body-Centric Radio Channels And Systems For Healthcare Applications," *IEEE Transactions on Information Technology in Biomedicine*, **16**, 2, 2012, pp. 221-227.

40. A. Sani, A. Alomainy and Y. Hao, "Numerical Characterization and Link Budget Evaluation of Wireless Implants Considering Different Digital Human Phantoms," *IEEE Transactions on Microwave Theory and Techniques, Biomedical Special Issue*, **57**, 10, 2009, pp. 2605-2613.

41. C. Miri et al., "Analysis of the Transmission Between On-Body Devices Using the Bilateral Dual-Grid FDTD Technique," *IEEE Antennas and Wireless Propagation Letters*, **9**, 2010, pp. 1073-1075.

42. Q. Wang, T. Tayamachi, I. Kimura and J. Wang, "An On-Body Channel Model for UWB Body Area Communications for Various Postures," *IEEE Transactions on Antennas and Propagation*, **AP-57**, 4, 2009, pp. 991-998.

43. A. Taflove, *Computational Electrodynamics: The Finite-Difference Time-Domain Method, Second Edition*, Norwood, MA, Artech House, 2000.

44. H. Hoteit, R. Sauleau, B. Philippe, Ph. Coquet and J.-P. Daniel, "Vector and Parallel Implementations for the FDTD Analysis of Millimeter Wave Planar Antennas," *International Journal of High Speed Computing*, **10**, 2, 1999, pp. 209-234.

45. A. Sani, Y. Hao, Y. Zhao, A. Alomainy and C. G. Parini, "An Efficient FDTD Algorithm Based on the Equivalence Principle for Analyzing On-Body Antenna Performance," *IEEE Transactions on Antennas and Propagation, Special Issue on Body-Centric Wireless Networks*, **AP-57**, 4, 2009, pp. 1006-1014.

46. Q. H. Abbasi, A. Sani, A. Alomainy and Y. Hao, "On-Body Radio Channel Characterization and System-Level Modeling for Multiband OFDM Ultra-Wideband Body-Centric Wireless Network," *IEEE Transactions on Microwave Theory and Techniques*, **58**, 12, 2010, pp. 3485- 3492.

47. A. Sani, Y. Hao, Y. Zhao, S.-L. Lee and G.-Z. Yang, "Subject-Specific Analysis Of The On-Body Radio Propagation Channel Adopting A Parallel FDTD Code," European Conference on Antennas and Propagation, Barcelona, 2010.

48. R. F. Harrington, *Field Computation by Moment Methods*, New York, Macmillan, 1968.

49. S. M. Rao, D. R. Wilton and A. W. Glisson, "Electromagnetic Scattering by Surfaces of Arbitrary Shape," *IEEE Transactions on Antennas and Propagation*, **AP-30**, 3, 1982, pp.409-418.

50. D.-S. Wang, "Limits and Validity of the Impedance Boundary Condition on Penetrable Surfaces," *IEEE Transactions on Antennas and Propagation*, **AP-35**, 4, 1987, pp. 453-457.

51. K. Ito, I. Ida and M.Wu, "Body Effect on Characteristics of Small Loop Antenna in Pager Systems," IEEE International Symposium on Antennas and Propagation, Chicago, 1992.

52. H. Chuang and W. Chen, "Computer Simulation of the Human-Body Effects on a Circular Loop-Wire Antenna for Radio-Pager Communications at 152, 280, and 400 MHz," *IEEE Transactions on Vehicular Technology*, **46**, 3, 1997, pp. 544-559.

53. D. Psychoudakis, G. Lee, C. Chen and J. Volakis, "Body-Worn Diversity Antennas for Squad Area Networks (SAN)," XXIX URSI General Assembly, Chicago, 2008.

54. D. Andreuccetti, R. Fossi and C. Petrucci, "Calculation of the Dielectric Properties of Body Tissues," http://niremf.ifac.cnr.it/tissprop.

55. N. Chahat, M. Zhadobov and R. Sauleau, and K. Ito, "A Compact UWB Antenna For On-Body Applications," *IEEE Transactions on Antennas and Propagation*, **AP-59**, 4, April 2011, pp. 1123-1131.

56. G. A. Conway and W. G. Scanlon, "Antennas for Over-Body-Surface Communication at 2.45 GHz," *IEEE Transactions on Antennas and Propagation*, **AP-57**, 4, April 2009, pp. 844-855.

57. J. Kim and Y. Rahmat-Samii, "Implanted Antennas Inside a Human Body: Simulations, Designs, and Characterizations," *IEEE Transactions on Microwave Theory and Techniques*, **52**, 8, 2004, pp. 1934-43.

58. S. Gabriel, R. W. Lau and C. Gabriel, "The Dielectric Properties of Biological Tissues: III. Parametric Models for the Dielectric Spectrum of Tissues," *Physics in Medicine and Biology*, **41**, 11, November 1996, pp. 2271-2293.

59. "IEEE Recommended Practice for Determining the Peak Spatial-Average Specific Absorption Rate (SAR) in the Human Head from Wireless Communication Devices: Measurement Techniques," IEEE Standard 1528-2003, 2003.

60. MCL Technologies, http://www.mcluk.org/.

61. A. W. Guy, "Analyses of Electromagnetic Fields Induced in Biological Tissues by Thermographic Studies on Equivalent Phantom Models," *IEEE Transactions on Microwave Theory and Techniques*, **19**, 2, February 1968, pp. 205-214.

62. K. Ito, K. Furuya, Y. Okano and L. Hamada, "Development and Characteristics of a Biological Tissue-Equivalent Phantom for Microwaves," *Electronic Communications in Japan Part I: Communications*, **84**, 4, April 2011, pp. 67-77.

63. Y. Okano, K. Ito and H. Kawai, "Solid Phantom Composed of Glycerin and its Applications to SAR Estimation," *IEICE Transactions on Communications*, **J38-B**, 4, 2000, pp. 534-54.

64. N. Chahat, M. Zhadobov, S. Alekseev and R. Sauleau, "Broadband Tissue-Equivalent Phantom for BAN Applications at Millimeter Waves," *IEEE Transactions on Microwave Theory and Techniques*, **60**, 7, July 2012, pp. 2259-2266.

65. N. Chahat, M. Zhadobov, S. Alekseev and R. Sauleau, "Human Skin-Equivalent Phantom for On-Body Antenna Measurements in 60 GHz Band," *Electronics Letters*, **48**, 2, January 2012, pp. 67-68.

66. N. Chahat, M. Zhadobov, R. Sauleau and S. I. Alekseev, "New Method for Determining Dielectric Properties of Skin and Phantoms at Millimeter Waves Based on Heating Kinetics," *Transactions on Microwave Theory and Techniques*, **60**, 3, March 2012, pp. 827-832.

67. M. Zhadobov, R. Augustine, R. Sauleau, S. Alekseev, A. Di Paola, C. Le Quément, Y. Soubere Mahamoud and Y. Le Dréan, "Complex Permittivity of Representative Biological Solutions in the 2-67 GHz Range," *Bioelectromagnetics*, **33**, 4, 2012, pp. 346-355.

68. Y. Nikawa, M. Chino and K. Kikuchi, "Soft and Dry Phantom Modeling Material Using Silicone Rubber with Carbon Fiber," *IEEE Transactions on Microwave Theory and Techniques*, **44**, 10, October 1996, pp. 1949-11952.

69. T. Kobayashi et al., "Dry Phantom Composed of Ceramics and its Applications to SAR Estimation," *IEEE Transactions on Microwave Theory and Techniques*, **41**, 1, January 1993, pp. 136-140.

70. J. T. Chang et al., "A Conductive Plastic for Simulating Biological Tissues at Microwave Frequencies," *IEEE Transactions of Electromagnetic Compatibility*, **39**, 2, May 1997, pp. 132-137.

71. The Visible Human Project, National Institute of Health, U.S. National Library of Medicine, http://www.nlm.nih.gov/research/visible/.

72. S.-L. Lee, K. Ali, A. Brizzi, J. Keegan, Y. Hao and G.-Z. Yang, "A Whole Body Statistical Shape Model for Radio Frequency Simulation," IEEE Engineering in Medicine and Biology Society Conference, Boston, 2011.

73. A. Christ et al., "The Virtual Family," *Physics and Medicine and Biology*, **55**, 23, 2010, pp. N23-N38.

74. Binvox, http://www.cs.princeton.edu/~min/binvox/.

75. P. S. Hall, et al., "Antennas and Propagation for On-Body Communication Systems," *IEEE Antennas and Propagation Magazine*, **49**, 3, June 2007, pp. 41-58.

76. Y. I. Nechayev, X. Wu, C. C. Constantinou and P. S. Hall, "Millimetre-Wave Path Loss Variability Between Two Body-Mounted Monopole Antennas," *IET Microwaves, Antennas and Propagation*, **7,** 1, January 2013, pp. 1-7.

77. A. Brizzi, A. Pellegrini, L. Zhang and Y. Hao, "Woodpile EBG-Based Antennas for Body Area Networks at 60 GHz," 4th High Speed Intelligent Communication Forum, Nanjing, 2012.

78. X. Y. Wu, L. Akhoondzadeh-Asl and P. S. Hall, "Printed Yagi-Uda Array for On-body Communication Channels at 60 GHz," *Microwave and Optical Technology Letters*, **53**, 12, December 2011, pp. 2728-2730.

79. X. Y. Wu and P. S. Hall, "Substrate Integrated Waveguide Yagi-Uda Antenna," *Electronic Letters*, **46**, 23, November 2010, pp. 1541-1542.

80. X. Y. Wu, Y. Nechayev and P. S. Hall, "Antenna Design and Channel Measurements for On-Body Communications at 60 GHz," XXX URSI General Assembly and Scientific Symposium of International Union of Radio Science, Turkey, August 2011.

81. N. Chahat, M. Zhadobov, L. Le Coq, S. I. Alekseev and R. Sauleau, "Characterization of the Interactions Between a 60-GHz Antenna and the Human Body in an Off-Body Scenario," *IEEE Transactions on Antennas and Propagation*, **AP-60**, 12, December 2012, pp. 5958-5965.

82. N. Chahat, M. Zhadobov, L. Le Coq and R. Sauleau, "Wearable Endfire Textile Antenna for On-Body Communications at 60 GHz," *IEEE Antennas and Wireless Propagation Letters*, **11**, 2012, pp. 799-802.

83. N. Chahat, M. Zhadobov, and R. Sauleau, "60-GHz Textile Antenna Array for Body-Centric Communications," *IEEE Transactions on Antennas Propagation*, **AP-61**, 4, April 2013, pp. 1816-1824.

84. G. V. Trentini, "Partially Reflecting Sheet Arrays," *IRE Transactions on Antennas and Propagation*, **4**, 4, 1956, 666-671.

85. Y. Lee, X. Lu, Y. Hao, S. Yang, J. R. G. Evans, C. G. Parini, "Narrow-Beam Azimuthally Omni-Directional Millimetre-Wave Antenna Using Freeformed Cylindrical Woodpile Cavity," *IET Microwave, Antennas and Propagation*, **4**, 10, 2010, pp. 1491-1499.

86. X. Lu, Y. Lee, S. Yang, Y. Hao, J. R. G. Evans, C. G. Parini and R. Ubic, "Fabrication of Electromagnetic Crystals by Extrusion Freeforming," *Metamaterials*, **2**, 1, 2008, pp. 36-44.

87. A. Brizzi, L. Zhang, A. Pellegrini and Y. Hao, "Design of a 60 GHz Metamaterial Antenna for Wireless BAN Applications," Advanced Electromagnetics Symposium, Paris, April 2012.

88. A. Brizzi, A. Pellegrini and Y. Hao, "Design of a Cylindrical Resonant Cavity Antenna for BAN Applications at V Band," IEEE International Workshop on Antenna Technology, Tucson, March 2012.

89. N. Chahat, G. Valerio, M. Zhadobov and R. Sauleau, "On-Body Propagation at 60 GHz," *IEEE Transactions on Antennas and Propagation*, AP-61, 4, April 2013, pp. 1876-188.

90. M. Zhadobov, Ch. N. Nicolaz, R. Sauleau, F. Desmots, D. Thouroude, D. Michel and Y. Le Dréan, "Evaluation of the Potential Biological Effects of Millimeter Waves At 60.42 GHz Upon Human Cells," *IEEE Transactions on Antennas and Propagation*, **AP-10**, 1, 2009, pp. 2949-2956.

91. M. Zhadobov, R. Sauleau, R. Augustine, C. Le Quément, Y. Le Dréan and D. Thouroude "Near-Field Dosimetry for In-Vitro Exposure of Human Cells at 60 GHz," *Bioelectromagnetics*, **33**, 1, 2012, pp. 55-64.

92. C. Le Quément, C. Nicolas Nicolaz, M. Zhadobov, F. Desmots, R. Sauleau, M. Aubry, D. Michel and Y. Le Dréan, "Whole-Genome Expression Analysis in Primary Human Keratinocyte Cell Cultures Exposed to 60 GHz Radiation," *Bioelectromagnetics*, **33**, 2, 2012, pp. 147-158.

93. K. Ali, A. Pellegrini, A. Brizzi, Y. Hao, "Full Wave and Ray-Based Analysis of a Body-Centric Scenario at V Band," European Conference on Antennas and Propagation, Gothenburg, 2013.